

# Output-feedback control of linear time-varying and nonlinear systems using the forward propagating Riccati equation

Journal of Vibration and Control  
2018, Vol. 24(7) 1239–1263  
© The Author(s) 2016  
Reprints and permissions:  
sagepub.co.uk/journalsPermissions.nav  
DOI: 10.1177/1077546316655913  
journals.sagepub.com/home/jvc  


Anna Prach<sup>1</sup>, Ozan Tekinalp<sup>2</sup> and Dennis S Bernstein<sup>3</sup>

## Abstract

For output-feedback control of linear time-varying (LTV) and nonlinear systems, this paper focuses on control based on the forward propagating Riccati equation (FPRE). FPRE control uses dual difference (or differential) Riccati equations that are solved forward in time. Unlike the standard regulator Riccati equation, which propagates backward in time, forward propagation facilitates output-feedback control of both LTV and nonlinear systems expressed in terms of a state-dependent coefficient (SDC). To investigate the strengths and weaknesses of this approach, this paper considers several nonlinear systems under full-state-feedback and output-feedback control. The internal model principle is used to follow and reject step, ramp, and harmonic commands and disturbances. The Mathieu equation, Van der Pol oscillator, rotational-translational actuator, and ball and beam are considered. All examples are considered in discrete time in order to remove the effect of integration accuracy. The performance of FPRE is investigated numerically by considering the effect of state and control weightings, the initial conditions of the difference Riccati equations, the domain of attraction, and the choice of SDC.

## Keywords

Nonlinear control, output feedback, Riccati equation, internal model principle, command following

## 1. Introduction

Output-feedback control of nonlinear systems is an extremely challenging problem of fundamental importance. In some applications, the assumption of linearity and the ability to measure all states can be satisfied to a sufficient extent that both aspects need not be dealt with simultaneously. In some applications, however, system nonlinearity cannot be ignored, and the available measurements are a strictly proper subset of the dominant states. In reality, all systems are nonlinear, and the inevitable presence of unmodeled dynamics means that the assumption of full-state feedback may be unrealistic in some applications.

From a theoretical point of view, output-feedback control of nonlinear systems remains a challenging and largely unsolved problem. The source of at least some of the difficulty stems from the lack of observer-regulator separation in the nonlinear case, although in some cases these difficulties can be overcome (Khalil, 2001; Arcaç, 2005). Separation aside, constructing

nonlinear observers and state estimators for nonlinear systems is itself a challenging problem that continues to attract considerable attention (Rajamani, 1998; Nijmeijer and Fossen, 1999; Julier and Uhlmann, 2004; Sauvage et al., 2007).

Among the available techniques for output-feedback control of nonlinear systems are passivity-based methods (Byrnes et al., 1991); however, passivity is often

<sup>1</sup>Singapore institute of Neurotechnology, National University of Singapore, Singapore

<sup>2</sup>Department of Aerospace Engineering, Middle East Technical University, Ankara, Turkey

<sup>3</sup>Department of Aerospace Engineering, University of Michigan, Ann Arbor, MI, USA

Received: 6 December 2015; accepted: 27 May 2016

### Corresponding author:

Anna Prach, Singapore Institute for Neurotechnology, 28 Medical Dr, Singapore 117456.  
Email: annaprach@me.com

violated in practice (Forbes and Damaren, 2010). Flatness-based techniques are also applicable assuming that multiple derivatives of the measurement can be obtained (van Nieuwstadt et al., 1998); however, sensor noise may render differentiation infeasible. Model predictive control techniques implemented with nonlinear observers provide another option (Findeisen et al., 2003; Mayne et al., 2006; Copp and Hespanha, 2014), assuming that separation is valid.

In view of the practical need for output-feedback control of nonlinear systems, the lack of rigorous techniques that are effective in practice has motivated interest in ad hoc methods. For example, gain-scheduling techniques based on local linearizations are widely used (Shamma and Athans, 1992). A closely related technique consists of parameterized linearizations in the form of linear parameter-varying (LPV) models (Scherer, 2001).

Another ad hoc class of nonlinear controllers is based on reformulating the nonlinear dynamics  $\dot{x}=f(x, u)$  in the ‘‘faux linearization’’ form  $\dot{x}=A(x)x+B(x)u$ , where  $A(x)$  and  $B(x)$  are state-dependent coefficients (SDC’s). By viewing the state  $x$  as instantaneously frozen, the state-dependent Riccati equation (SDRE) approach solves the regulator algebraic Riccati equation at each point in time (Mracek and Cloutier, 1998; Shamma and Cloutier, 2003; Erdem and Alleyne, 2004; Banks et al., 2007; Cimen, 2010; Korayem and Nekoo, 2015). The regulator gain can then be used in a separation structure by solving the dual estimator algebraic Riccati equation with the argument  $x$  of the SDC’s  $A(x)$  and  $B(x)$  replaced by the state estimate  $\hat{x}$  (Mracek et al., 1996; Chandrasekhar et al., 2005).

A variation of SDRE is to replace the algebraic Riccati equations with differential Riccati equations. For the estimator, this presents no difficulty since the Kalman filter propagates forward in time. The only distinction is the use of the state-dependent coefficient  $A(\hat{x})$  in place of the Jacobian used in the extended Kalman filter. For the regulator, however, the optimal gain is obtained by propagating the differential Riccati equation backward in time (Callier et al., 1994). Unfortunately, this is not feasible for nonlinear systems due to the fact that the future state estimate is not known.

To overcome the problem of backward propagation of the differential regulator Riccati equation and the need to know the future state estimate, a *forward-propagating Riccati equation* (FPRE) technique is proposed in Chen and Kao (1997), Weiss et al. (2012), Prach et al. (2014a) and Prach et al. (2014b). The idea behind this approach is to remove the minus sign in the backward-propagating regulator Riccati equation and propagate the equation forward as in

the case of the differential estimator Riccati equation. This technique is rigorously analyzed and fully justified in Prach et al. (2015) within the context of linear time-invariant (LTI) systems. However, like SDRE control, FPRE is not guaranteed to be stabilizing or optimal for nonlinear systems. Nevertheless, when combined with the dual estimator whose coefficients depend on the state estimates, FPRE provides a potentially useful technique for output-feedback control of nonlinear systems that can be cast in SDC form Prach et al. (2014b).

A related application of FPRE is control of linear time-varying (LTV) systems without future knowledge of the system matrices (Weiss et al., 2012; Prach et al., 2014a). If  $A(t)$  and  $B(t)$  are known in advance, then classical optimal control methods can be used over a finite horizon. If  $A(t)$  and  $B(t)$  are known over a limited future interval and the objective is stabilization, then receding horizon techniques can be used Tadmor (1992). For periodically time-varying systems, stabilization is considered in Bittanti and Colaneri (2009). However, in many applications, knowledge of the future dynamics is not available. This is the case for LPV models, where  $A(\rho(t))$  and  $B(\rho(t))$  depend on a time-varying parameter  $\rho(t)$  whose future time variation is not known. FPRE thus provides an alternative approach to controlling LPV systems.

For LTV systems, the theoretical challenge of FPRE stems from the fact that the differential regulator Riccati equation is not guaranteed to be stabilizing. For the case of the differential estimator Riccati equation, a quadratic Lyapunov function can be used to guarantee stability, and this provides the foundation for the stability of the Kalman filter when used as an observer for LTV systems (Afanas’ev et al., 1996; Crassidis and Junkins, 2004; Weiss et al., 2012). For the differential regulator Riccati equation, the analogous technique does not yield stability due to the fact that the time-varying matrices  $A(t)$  and  $C(t)$  are replaced by the dual time-varying matrices  $A^T(t)$  and  $B^T(t)$ , respectively. In the LTI case, this replacement causes no difficulties since the spectra of  $A-FC$  and  $(A-FC)^T$  are identical. As shown in Weiss et al. (2012), however, asymptotic stability of the state transition matrix of  $A(t)-F(t)C(t)$  does not imply asymptotic stability of the state transition matrix of  $(A(t)-F(t)C(t))^T$ . Consequently, for LTV systems, there is no guarantee of stability through a duality argument. For nonlinear systems, the use of the state-estimate-dependent coefficient  $A(\hat{x}(t))$  presents an additional challenge.

The contribution of the present paper is a numerical investigation of FPRE aimed at assessing the viability and efficacy of this method for output-feedback control of LTV and nonlinear systems. To do this, we consider a collection of systems that have been widely considered in the literature using alternative methods.

These systems include the two-mass system, Mathieu equation, Van der Pol oscillator, ball and beam, and rotational-translational actuator. For each problem, the goal is to determine the performance of FPRE under output feedback. For example, for the ball-and-beam system, full-state-feedback control laws are derived in Hauser et al. (1992), Barbuand et al. (1997) and Teel (1992), while output-feedback control laws are considered in Teel (1993). Likewise, for the rotational-translational actuator (RTAC), full-state-feedback control laws are derived in Bupp et al. (1998), Jankovic et al. (1996) and Tadmor (2001), and an observer-based controller using dissipativity techniques is given in Tadmor (2001).

We consider step, ramp, and harmonic commands and disturbances under full-state-feedback and output-feedback control. To achieve simultaneous command following and disturbance rejection for this class of signals, we apply the internal model principle (IMP), which states that asymptotic command following and disturbance rejection require a model of the exogenous signals in the feedback loop (Isidori et al., 2003). The most basic example of IMP in linear feedback control of LTI systems is the fact that an integrator in the controller is needed to reject step disturbances, whereas an integrator in either the system or the controller suffices to follow step commands. Both statements are consequences of the final value theorem, while analogous statements apply to ramp and harmonic disturbances and commands. Since the final value theorem is valid for only LTI systems, the purpose of this analysis is to motivate a suitable feedback control architecture for use with LTV and nonlinear systems. The fundamental importance of IMP is reflected by its extensive application to linear controller synthesis (Johnson, 1971; Young and Willems, 1972; Francis et al., 1974; Davison and Goldenberg, 1975; Francis and Wonham, 1975; Hoagg et al., 2008). Within the context of nonlinear feedback control, IMP is developed in Byrnes and Isidori (2003) and Isidori (1995).

In this study, we investigate the performance of FPRE under various choices of controller tuning parameters. These parameters include the state and control weightings, the initial conditions of the forward-propagating Riccati equations, and the choice of the SDC matrices. We also vary the initial conditions of the system in order to estimate the domain of attraction of FPRE and its dependence on the convergence of the state of the observer-based compensator. These numerical investigations are intended to highlight the strengths and weaknesses of FPRE control for LTV and nonlinear systems while motivating future theoretical developments.

The examples considered in this paper are chosen to demonstrate the flexibility aspects of FPRE. The two-mass system demonstrates IMP-based control with output feedback. This example defines the feedback

control architecture for all subsequent examples. Next, the Mathieu equation is a second-order LTV system that has been extensively analyzed by Richards (1983). Command following and disturbance rejection are demonstrated for this system using output feedback. A notable aspect of FPRE is its ability to stabilize the Mathieu equation, which is unstable for certain frequencies and amplitudes of the sinusoidal stiffness. This ability has not previously been demonstrated under output feedback.

The three nonlinear examples are chosen to demonstrate additional challenges to output-feedback control of nonlinear systems. The Van der Pol oscillator is a self-excited system, and thus stabilization is required to suppress the limit cycle. Stabilization, command following, and disturbance rejection are demonstrated for this system using output feedback. This ability has not previously been demonstrated. The RTAC has been extensively studied, but exclusively under either full-state or passivity assumptions. In the present paper, we consider simultaneous command following and disturbance rejection under output feedback. This study quantifies the achievable command-following performance in terms of the frequency and amplitude of the harmonic command. The RTAC also provides a useful venue for exploring the effect of the choice of SDC on FPRE performance. Finally, the ball and beam provides a severe challenge to stabilization due to the fact that its linearization is a quadruple integrator. Unlike prior treatments of this system, which assume both full-state feedback and no disturbance, we consider simultaneous command following and disturbance rejection without full-state measurements. In all of these cases (simultaneous command following and disturbance rejection for LTV and nonlinear systems with output-feedback control), we are not aware of comparable treatments in the literature by any method.

## 2. Command following and disturbance rejection for LTI SISO systems: Full-state-feedback case

Consider the discrete-time LTI system

$$x_{k+1} = Ax_k + Bu_k + D_1d_k \quad (1)$$

$$y_{r,k} = Hx_k \quad (2)$$

where  $x_k \in \mathbb{R}^n$ ,  $u_k \in \mathbb{R}$ ,  $d_k \in \mathbb{R}$ ,  $y_{r,k} \in \mathbb{R}$ ,  $A \in \mathbb{R}^{n \times n}$ ,  $B \in \mathbb{R}^n$ ,  $D_1 \in \mathbb{R}^n$ , and  $H \in \mathbb{R}^{1 \times n}$ . For full-state-feedback control, we assume that  $x_k$  is measured. Let  $r_k \in \mathbb{R}$  be the command, and define the command-following error

$$z \triangleq r - y_r \quad (3)$$

The signals  $r$  and  $d$  are assumed to be linear combinations of steps, ramps, and sinusoids. The goal is to have the command-following error  $z$  converge to zero in the presence of the disturbance  $d$ . This goal is facilitated by an internal model of the command  $r$  and disturbance  $d$  of the form

$$x_{im,k+1} = A_{im}x_{im,k} + B_{im}z_k \tag{4}$$

where  $x_{im,k} \in \mathbb{R}^{n_{im}}$  is the state of the internal model.

Figure 1 shows the internal-model-based full-state-feedback control architecture, where  $G$  is the transfer function of the system (1),  $G_{im}$  is the transfer function of the internal model (4), and  $K_{im}$  and  $K$  are full-state-feedback gains. These components are described in more detail below.

Augmenting (1), (2) with (4) yields

$$x_{a,k+1} = A_a x_{a,k} + B_a u_k + \begin{bmatrix} 0_{n \times 1} \\ B_{im} \end{bmatrix} r_k + \begin{bmatrix} D_1 \\ 0_{n_{im} \times 1} \end{bmatrix} d_k \tag{5}$$

where

$$\begin{aligned} x_{a,k} &\triangleq \begin{bmatrix} x_k \\ x_{im,k} \end{bmatrix}, & A_a &\triangleq \begin{bmatrix} A & 0_{n \times n_{im}} \\ -B_{im}H & A_{im} \end{bmatrix} \\ B_a &\triangleq \begin{bmatrix} B \\ 0_{n_{im} \times 1} \end{bmatrix} \end{aligned} \tag{6}$$

Defining  $u_{im} \triangleq K_{im}x_{im}$ , the control  $u$  is given by

$$u_k = K_a x_{a,k} = Kx_k + K_{im}x_{im,k} = Kx_k + u_{im,k} \tag{7}$$

where  $K_a = [K \ K_{im}] \in \mathbb{R}^{m \times (n+n_{im})}$  is the full-state-feedback gain.

### 2.1. Algebraic Riccati equation control law

For algebraic Riccati equation (ARE) control, we consider the cost

$$J(u) = \sum_{k=0}^{\infty} (x_{a,k}^T R_1 x_{a,k} + R_2 u_k^2) \tag{8}$$

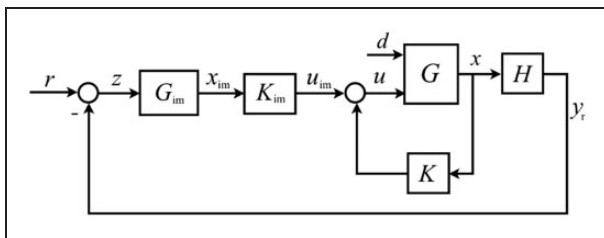


Figure 1. Internal-model-based, full-state-feedback controller.

where  $R_1 \in \mathbb{R}^{(n+n_{im}) \times (n+n_{im})}$  is positive semidefinite and  $R_2$  is a positive number. The optimal constant feedback gain  $K_a$  is given by

$$K_a = -(B_a^T \bar{P}_a B_a + R_2)^{-1} B_a^T \bar{P}_a A_a \tag{9}$$

where  $\bar{P}_a \in \mathbb{R}^{(n+n_{im}) \times (n+n_{im})}$  satisfies the ARE

$$\begin{aligned} \bar{P}_a &= A_a^T \bar{P}_a A_a - A_a^T \bar{P}_a B_a (B_a^T \bar{P}_a B_a + R_2)^{-1} B_a^T \bar{P}_a A_a \\ &\quad + R_1 \end{aligned} \tag{10}$$

### 2.2. Forward propagating Riccati equation (FPRE) control law

For FPRE control, the constant feedback gain (9) is replaced by the time-varying feedback gain

$$K_{a,k} = -(B_a^T P_{a,k} B_a + R_2)^{-1} B_a^T P_{a,k} A_a \tag{11}$$

where  $P_{a,k} \in \mathbb{R}^{(n+n_{im}) \times (n+n_{im})}$  satisfies the difference Riccati equation

$$\begin{aligned} P_{a,k+1} &= A_a^T P_{a,k} A_a \\ &\quad - A_a^T P_{a,k} B_a (B_a^T P_{a,k} B_a + R_2)^{-1} B_a^T P_{a,k} A_a + R_1 \end{aligned} \tag{12}$$

with the positive-semidefinite initial condition  $P_{a,0}$ , where  $R_1 \in \mathbb{R}^{(n+n_{im}) \times (n+n_{im})}$  is positive semidefinite and  $R_2$  is a positive number.

The solution  $P_{a,k}$  of (12) converges exponentially to  $\bar{P}_a$ . This is illustrated numerically in Example 1 and proved in Prach et al. (2015) for the continuous-time case. Because knowledge of the future dynamics is not needed, FPRE control will be used in later sections for LTV and nonlinear systems.

### 2.3. Convergence analysis

We use the final value theorem to analyze the convergence of the error  $z$  for the internal-model-based full-state-feedback controller in the case where  $K_a$  is constant. Although this treatment is classical, the goal is to set the stage for the later application to LTV and nonlinear systems. Consider the reformulation of Figure 1 shown in Figure 2, where  $G_c$  is the transfer function of the internal model with the feedback gain  $K_{im}$ , that is

$$G_c(z) \triangleq K_{im}(zI - A_{im})^{-1} B_{im} \tag{13}$$

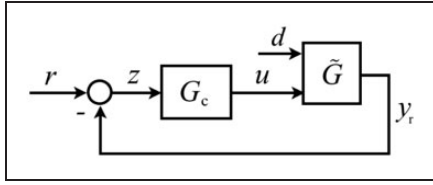


**Figure 2.** Reformulation of Figure 1 for analysis based on the final value theorem.

and  $\tilde{G} \triangleq [G_u \ G_d]$  is the transfer function of (1), (2) from  $[u \ d]^T$  to  $y_r$  with the feedback gain  $K$ , where

$$G_u(z) \triangleq (zI - (A + BK))^{-1} B \quad (14)$$

$$G_d(z) \triangleq (zI - (A + BK))^{-1} D_1 \quad (15)$$

Let  $\hat{r}$  denote the  $z$ -transform of  $r$ , and similarly for other signals. Then

$$\hat{z} = \hat{r} - \hat{y}_r, \quad \hat{y}_r = \tilde{G} \begin{bmatrix} \hat{u} \\ \hat{d} \end{bmatrix} = G_u \hat{u} + G_d \hat{d} \quad (16)$$

Thus

$$\hat{z} = \hat{r} - G_u \hat{u} - G_d \hat{d} = \hat{r} - G_u G_c \hat{z} - G_d \hat{d} \quad (17)$$

and (17) can be written as

$$\hat{z} = \frac{1}{1 + G_u G_c} \hat{r} - \frac{G_d}{1 + G_u G_c} \hat{d} \quad (18)$$

Let  $G_u = \frac{N_u}{D_u}$  and  $G_c = \frac{N_c}{D_c}$ , note that  $G_d = \frac{N_d}{D_u}$ , and let  $\hat{r} = \frac{n_r}{d_r}$  and  $\hat{d} = \frac{n_d}{d_d}$ . Then

$$\hat{z} = \frac{D_u D_c}{D_u D_c + N_u N_c} \frac{n_r}{d_r} - \frac{D_c N_d}{D_u D_c + N_u N_c} \frac{n_d}{d_d} \quad (19)$$

Next, since (4) is an internal model of  $r$  and  $d$ , it follows that internal models of the command  $r$  and disturbance  $d$  are present in the denominator  $D_c$  of  $G_c$ . Therefore,  $D_c = \tilde{d}_r d_r = \tilde{d}_d d_d$ , where  $\tilde{d}_r$  and  $\tilde{d}_d$  are polynomials, and thus

$$\hat{z} = \frac{D_u \tilde{d}_r n_r}{D_u D_c + N_u N_c} - \frac{\tilde{d}_d N_d n_d}{D_u D_c + N_u N_c} \quad (20)$$

Assuming that  $D_u D_c + N_u N_c$  is asymptotically stable, the final value theorem yields

$$\begin{aligned} \lim_{k \rightarrow \infty} z_k &= \lim_{z \rightarrow 1} (z - 1) \hat{z} \\ &= \lim_{z \rightarrow 1} \left[ \frac{(z - 1) D_u \tilde{d}_r n_r}{D_u D_c + N_u N_c} - \frac{(z - 1) \tilde{d}_d N_d n_d}{D_u D_c + N_u N_c} \right] \\ &= 0 \end{aligned} \quad (21)$$

## 2.4. Internal models

For the case where the command and disturbance are steps, the internal model is an integrator given by

$$A_{im} = 1, \quad B_{im} = 1, \quad C_{im} = 1 \quad (22)$$

For the case where the command and disturbance are ramps, the internal model is a double integrator given by

$$A_{im} = \begin{bmatrix} 0 & 1 \\ -1 & 2 \end{bmatrix}, \quad B_{im} = \begin{bmatrix} 0 \\ 1 \end{bmatrix}, \quad C_{im} = [1 \ 0] \quad (23)$$

For the case where the command and disturbance are harmonic with the same frequency  $\Omega$ , the internal model is an undamped oscillator with frequency  $\Omega$  given by

$$\begin{aligned} A_{im} &= \begin{bmatrix} 0 & 1 \\ -1 & 2 \cos(\Omega) \end{bmatrix}, \quad B_{im} = \begin{bmatrix} 0 \\ 1 \end{bmatrix}, \\ C_{im} &= [1 \ 0] \end{aligned} \quad (24)$$

The matrix  $C_{im}$  is used for output feedback, but is not needed for full-state feedback.

If the command and disturbance are harmonic with frequencies  $\Omega_1$  and  $\Omega_2$ , respectively, then the internal model is fourth-order and consists of the cascade of two undamped oscillators with frequencies  $\Omega_1$  and  $\Omega_2$ . Likewise, if the command is a step and the disturbance is harmonic with frequency  $\Omega$  (or vice versa), then the internal model is third-order and consists of the cascade of an integrator and an undamped oscillator with frequency  $\Omega$ .

In internal-model-based control, neither the height of a step command or step disturbance nor the amplitude or phase shift of a harmonic command or disturbance need to be known. However, the frequencies of a harmonic command and a harmonic disturbance must be known. This is a standard requirement in control based on the internal model principle.

## 2.5. Discrete-time models

Each example in this paper is based on a continuous-time model. In order to obtain discrete-time models for feedback control, we apply Euler integration to the continuous-time system. For each example,  $T_s$  is chosen sufficiently small that the open-loop unit step response of the Euler-discretized model is numerically close to the open-loop step response of the continuous-time model computed by the Matlab routine ODE45. In order to remove the issue of integration accuracy from the numerical investigation, the Euler-discretized model is then viewed as the truth model for control, and the performance of each control law is considered

only within the context of the discretized model. Evaluation of the performance of the control laws on the underlying continuous-time system is outside the scope of this paper.

Consider the continuous-time system

$$\dot{x}(t) = A_{\text{cont}}x(t) + B_{\text{cont}}u(t) + D_{1,\text{cont}}d(t) \quad (25)$$

$$y(t) = C_{\text{cont}}x(t) \quad (26)$$

Using Euler integration, we obtain the discrete-time version of (25), (26) given by

$$x_{k+1} = x_k + T_s A_{\text{cont}}x_k + T_s B_{\text{cont}}u_k + T_s D_{1,\text{cont}}d_k \quad (27)$$

$$y_k = C_{\text{cont}}x_k \quad (28)$$

where  $T_s$  is the sample time,  $x_k \triangleq x(kT_s)$ ,  $u_k \triangleq u(kT_s)$ ,  $d_k \triangleq d(kT_s)$ , and  $y_k \triangleq y(kT_s)$ . Then, the discrete-time matrices  $A$ ,  $B$ ,  $C$ ,  $D_1$  are given by

$$\begin{aligned} A &= I + T_s A_{\text{cont}}, & B &= T_s B_{\text{cont}} \\ C &= C_{\text{cont}}, & D_1 &= T_s D_{1,\text{cont}} \end{aligned} \quad (29)$$

### 2.6. Example 1. Full-state-feedback control of the two-mass system with harmonic command and harmonic disturbance

Consider the continuous-time LTI system in Figure 3, which represents masses  $m_1$  and  $m_2$  connected by a spring with stiffness  $k$  and dashpot with damping  $b$ . The control force  $f$  is applied to  $m_2$ , and the goal is to command the position  $q_1$  of  $m_1$ . We consider the case of an unmatched disturbance, where the disturbance  $d$  is applied to  $m_1$  as shown in Figure 3.

The equations of motion are given by

$$m_1 \ddot{q}_1 + b(\dot{q}_1 - \dot{q}_2) + k(q_1 - q_2) = d \quad (30)$$

$$m_2 \ddot{q}_2 + b(\dot{q}_2 - \dot{q}_1) + k(q_2 - q_1) = f \quad (31)$$

For the state vector  $x \triangleq [q_1 \ \dot{q}_1 \ q_2 \ \dot{q}_2]^T$ , the continuous-time matrices in (25) are given by

$$\begin{aligned} A_{\text{cont}} &= \begin{bmatrix} 0 & 1 & 0 & 0 \\ -\frac{k}{m_1} & -\frac{b}{m_1} & \frac{k}{m_1} & \frac{b}{m_1} \\ 0 & 0 & 0 & 1 \\ \frac{k}{m_2} & \frac{b}{m_2} & -\frac{k}{m_2} & -\frac{b}{m_2} \end{bmatrix} \\ B_{\text{cont}} &= \begin{bmatrix} 0 \\ 0 \\ 0 \\ 1 \end{bmatrix}, & D_{1,\text{cont}} &= \begin{bmatrix} 0 \\ 1 \\ 0 \\ 0 \end{bmatrix} \end{aligned} \quad (32)$$

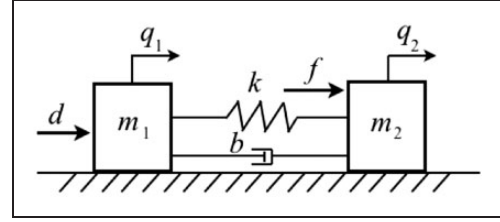


Figure 3. Example 1. The disturbance  $d$  is unmatched.

We let  $T_s = 0.1$  s, and use (29) to obtain discrete-time matrices  $A$ ,  $B$ ,  $D_1$ .

To command the position  $q_1$  of mass  $m_1$ , let  $y_r = q_1$ . Let  $m_1 = 1$  kg,  $m_2 = 0.5$  kg,  $k = 2$  N/m,  $b = 0.3$  N-s/m, and  $x_0 = [0.2 \text{ m}, 0 \text{ m/s}, -0.1 \text{ m}, 0 \text{ m/s}]^T$ . For these parameters, the damped natural frequency is 2.45 rad/s, and the damping ratio is 7.5%.

Consider the harmonic command  $r_k = 0.5 \sin(\Omega_1 k)$  m and the harmonic disturbance  $d_k = \cos(\Omega_2 k)$  N, with  $\Omega_1 = 0.1$  rad/sample and  $\Omega_2 = 0.5$  rad/sample. For  $T_s = 0.1$  s, these discrete-time frequencies correspond to the continuous-time frequencies 1 rad/s and 5 rad/s, respectively. The internal model is given by the cascade of two undamped oscillators (24) whose frequencies are equal to the frequencies of the command and disturbance.

Let  $R_1 = I_5$ ,  $R_2 = 1$ , and  $P_{a,0} = I_{n+n_m}$ . Figure 4 shows the closed-loop response, and Figure 5 shows the convergence of  $P_{a,k}$  of FPRE to  $\bar{P}_a$  of ARE.

### 3. Internal-model-based command following and disturbance rejection: Output-feedback case

Consider the LTI system (1). Let  $y_{r,k} \triangleq Hx_k$  and  $y_k \triangleq Cx_k$ , and define the measurement vector

$$\begin{aligned} y_{\text{meas},k} &= \begin{bmatrix} y_{r,k} \\ y_k \end{bmatrix} + D_2 v_k \\ &= \begin{bmatrix} Hx_k \\ Cx_k \end{bmatrix} + D_2 v_k = C_{\text{meas}}x_k + D_2 v_k \end{aligned} \quad (33)$$

where  $v_k \in \mathbb{R}^m$  is vector of zero-mean white noise with covariance  $I_m$ ,  $C_{\text{meas}} \in \mathbb{R}^{m \times n}$ ,  $H \in \mathbb{R}^{1 \times n}$ ,  $C \in \mathbb{R}^{(m-1) \times n}$ , and  $D_2 \in \mathbb{R}^{m \times m}$ . If only one measurement is available, then  $y_{\text{meas}} = y_r + D_2 v_k$  and  $C$  is absent. Except for Example 3, sensor noise is omitted from the simulations. However, the sensor-noise covariance  $V_2 \triangleq D_2 D_2^T \in \mathbb{R}^{m \times m}$  is used as a design parameter by FPRE. The command-following error is defined by (3).

Figure 6 shows the internal-model-based output-feedback control architecture, where  $G$  is the transfer function of the system (1), (33),  $G_{\text{im}}$  is the transfer

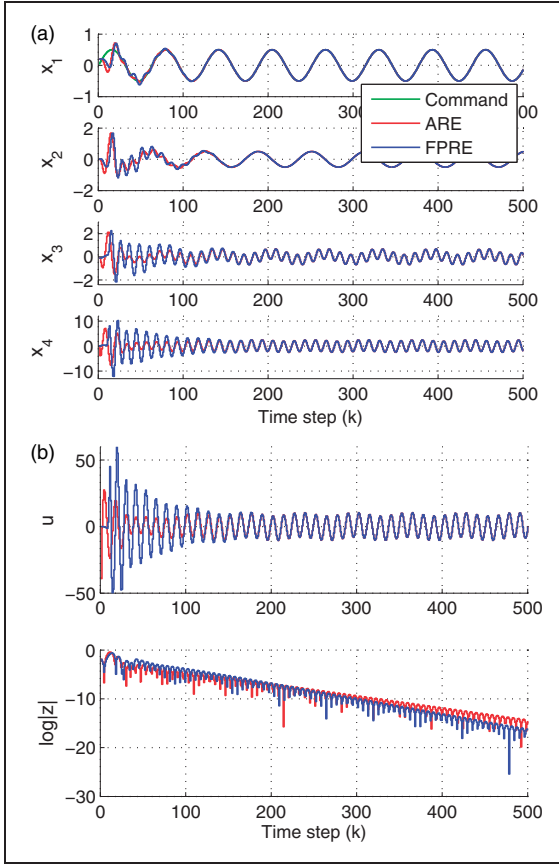


**Figure 4.** Example I. Internal-model-based, full-state-feedback control of the two-mass system: (a) state trajectories; (b) control input and command-following error. The command and disturbance are harmonic with amplitudes 0.5 m and 1.0 N, respectively, and with frequencies 0.1 rad/sample and 0.5 rad/sample, respectively.

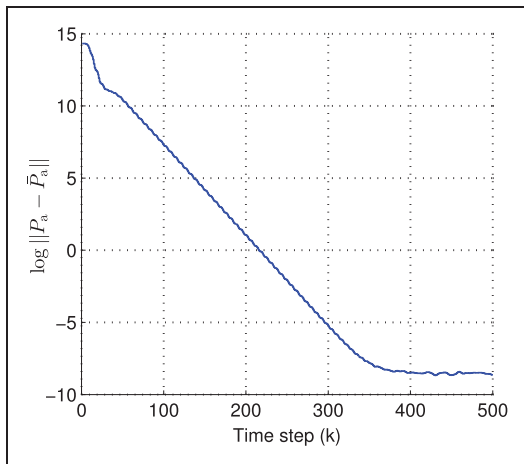


**Figure 5.** Example I. Internal-model-based, full-state-feedback control of the two-mass system. This plot shows exponential convergence of  $P_{a,k}$  of FPFE to  $\bar{P}_a$  of ARE. The norm is the maximum singular value.

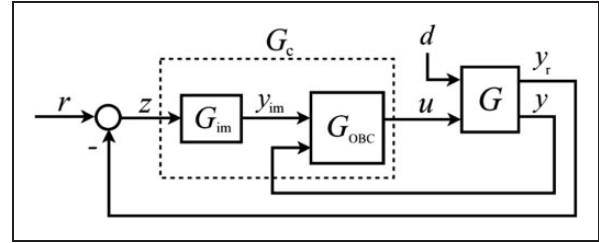


**Figure 6.** Internal-model-based output-feedback controller.

function of the internal model,  $G_{OBC}$  is the transfer function of the observer-based compensator, and  $G_c$  is the transfer function of the augmented compensator. These components are described below.

We augment (1), (33) with the SISO internal model

$$x_{im,k+1} = A_{im}x_{im,k} + B_{im}z_k \quad (34)$$

$$y_{im,k} = C_{im}x_{im,k} \quad (35)$$

where  $x_{im} \in \mathbb{R}^{n_{im}}$ . The augmented system is thus given by

$$x_{a,k+1} = A_a x_{a,k} + B_a u_k + \begin{bmatrix} 0_{n \times 1} \\ B_{im} \end{bmatrix} r_k + \begin{bmatrix} D_1 \\ 0_{n_{im} \times 1} \end{bmatrix} d_k \quad (36)$$

$$y_{a,k} = C_a x_{a,k} \quad (37)$$

where

$$x_{a,k} \triangleq \begin{bmatrix} x_k \\ x_{im,k} \end{bmatrix} \in \mathbb{R}^{n+n_{im}}, \quad y_{a,k} \triangleq \begin{bmatrix} y_k \\ y_{im,k} \end{bmatrix} \in \mathbb{R}^{m-1+n_{im}},$$

$$A_a \triangleq \begin{bmatrix} A & 0_{n \times n_{im}} \\ -B_{im}H & A_{im} \end{bmatrix}, \quad B_a \triangleq \begin{bmatrix} B \\ 0_{n_{im} \times 1} \end{bmatrix}$$

$$C_a \triangleq \begin{bmatrix} C & 0_{(m-1) \times n_{im}} \\ 0_{1 \times n} & C_{im} \end{bmatrix} \quad (38)$$

A block diagram of the augmented system (36), (37) is shown in Figure 7.

Next, for the augmented system (36), (37), we use the observer-based compensator

$$\hat{x}_{a,k+1} = (A_a + B_a K_a - F_a C_a) \hat{x}_{a,k} + F_a y_{a,k} \quad (39)$$

$$u_k = K_a \hat{x}_{a,k} \quad (40)$$

where  $\hat{x}_{a,k} \in \mathbb{R}^{n+n_{im}}$  and  $F_a \in \mathbb{R}^{(n+n_{im}) \times m}$ . For ARE control, the constant regulator feedback gain  $K_a$  is given by (9), whereas, for FPFE control, the time-varying regulator feedback gain  $K_{a,k}$  is given by (11). The constant observer gain  $F_a$  for ARE control, as well as the

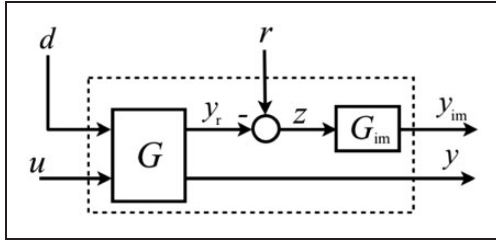


Figure 7. Augmented system.

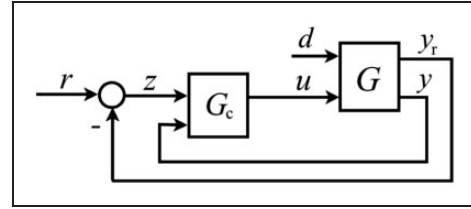


Figure 8. Reformulation of Figure 6 for analysis based on the final value theorem.

time-varying observer gain  $F_{a,k}$  for FPRE control, are defined below.

### 3.1. ARE observer-based compensator

For ARE control, the constant observer gain  $F_a$  is given by

$$F_a = A_a \bar{Q}_a C_a^T (C_a \bar{Q}_a C_a^T + V_2)^{-1} \quad (41)$$

where  $\bar{Q} \in \mathbb{R}^{(n+n_{im}) \times (n+n_{im})}$  satisfies

$$\begin{aligned} \bar{Q}_a = & A_a \bar{Q}_a A_a^T - A_a \bar{Q}_a C_a^T (C_a \bar{Q}_a C_a^T + V_2)^{-1} C_a \bar{Q}_a A_a^T \\ & + V_1 \end{aligned} \quad (42)$$

where  $V_1 \in \mathbb{R}^{(n+n_{im}) \times (n+n_{im})}$  is positive semidefinite and  $V_2 \in \mathbb{R}^{m \times m}$  is positive definite.

### 3.2. FPRE observer-based compensator

For FPRE control, the time-varying observer gain  $F_{a,k}$  is given by

$$F_{a,k} = A_a Q_{a,k} C_a^T (C_a Q_{a,k} C_a^T + V_2)^{-1} \quad (43)$$

where  $Q_{a,k} \in \mathbb{R}^{(n+n_{im}) \times (n+n_{im})}$  satisfies

$$\begin{aligned} Q_{a,k+1} = & A_a Q_{a,k} A_a^T \\ & - A_a Q_{a,k} C_a^T (C_a Q_{a,k} C_a^T + V_2)^{-1} C_a Q_{a,k} A_a^T + V_1 \end{aligned} \quad (44)$$

with the positive-semidefinite initial condition  $Q_{a,0}$ , where  $V_1 \in \mathbb{R}^{(n+n_{im}) \times (n+n_{im})}$  is positive semidefinite and  $V_2 \in \mathbb{R}^{m \times m}$  is positive definite.

We cascade the observer-based compensator (39), (40) with the internal model (34), (35) to obtain the augmented compensator

$$x_{c,k+1} = A_c x_{c,k} + B_c z_k + \begin{bmatrix} F_a \\ 0_{n_{im} \times (m-1)} \end{bmatrix} \begin{bmatrix} y_k \\ 0_{1 \times 1} \end{bmatrix} \quad (45)$$

$$u_k = C_c x_{c,k} \quad (46)$$

where

$$\begin{aligned} x_{c,k} &\triangleq \begin{bmatrix} \hat{x}_{a,k} \\ x_{im,k} \end{bmatrix} \in \mathbb{R}^{n+2n_{im}} \\ A_c &\triangleq \begin{bmatrix} A_a + B_a K_a - F_a C_a & F_a C_{im} \\ 0_{n_{im} \times (n+n_{im})} & A_{im} \end{bmatrix} \\ B_c &\triangleq \begin{bmatrix} 0_{(n+n_{im}) \times 1} \\ B_{im} \end{bmatrix}, C_c \triangleq [K_a \quad 0_{1 \times n_{im}}] \end{aligned} \quad (47)$$

If the only measurement is  $y_r$ , then the last term in (45) is absent.

### 3.3. Convergence analysis

Consider the reformulation of Figure 6 shown in Figure 8, where

$$G \triangleq \begin{bmatrix} G_{y,u} & G_{y,d} \\ G_{y,u} & G_{y,d} \end{bmatrix}$$

is the transfer function of the system (1), (35), where

$$\begin{aligned} G_{y,u}(z) &\triangleq H(zI - A)^{-1} B, \quad G_{y,d}(z) \triangleq H(zI - A)^{-1} D \\ G_{yu}(z) &\triangleq C(zI - A)^{-1} B, \quad G_{yd}(z) \triangleq C(zI - A)^{-1} D_1 \end{aligned} \quad (48)$$

and  $[y_r \ y]^T = G[u \ d]^T$ . Furthermore,  $G_c \triangleq [G_{cz} \ G_{cy}]$  is the transfer function of the augmented compensator (45), (46), where  $u = G_c[z \ y]^T$  and

$$\begin{aligned} G_{cz}(z) &\triangleq C_c(zI - A_c)^{-1} B_c \\ G_{cy}(z) &\triangleq C_c(zI - A_c)^{-1} \begin{bmatrix} F_a \\ 0_{n_{im} \times (m-1)} \end{bmatrix} \end{aligned} \quad (49)$$

Since

$$\hat{z} = \hat{r} - \hat{y}_r, \quad \hat{y}_r = G_{y,u} \hat{u} + G_{y,d} \hat{d} \quad (50)$$

it follows that

$$\begin{aligned}\hat{z} &= \hat{r} - G_{y_r,u}\hat{u} - G_{y_r,d}\hat{d} \\ &= \hat{r} - G_{y_r,u}G_{cz}\hat{z} - G_{y_r,u}G_{cy}\hat{y} - G_{y_r,d}\hat{d}\end{aligned}\quad (51)$$

Since

$$\begin{aligned}\hat{y} &= G_{y_u}\hat{u} + G_{y_d}\hat{d} \\ &= G_{y_u}G_{cz}\hat{z} + G_{y_u}G_{cy}\hat{y} + G_{y_d}\hat{d}\end{aligned}\quad (52)$$

(52) implies that

$$\hat{y} = \Phi_{yz}\hat{z} + \Phi_{yd}\hat{d}\quad (53)$$

where

$$\Phi_{yz} \triangleq \frac{G_{y_u}G_{cz}}{1 - G_{y_u}G_{cy}}, \quad \Phi_{yd} \triangleq \frac{G_{y_d}}{1 - G_{y_u}G_{cy}}\quad (54)$$

Using (53), (51) can be written as

$$\begin{aligned}\hat{z} &= \hat{r} - G_{y_r,u}(G_{cz}\hat{z} + G_{cy}\Phi_{yz})\hat{z} \\ &\quad - (G_{y_r,u}G_{cy}\Phi_{yd} + G_{y_r,d})\hat{d}\end{aligned}\quad (55)$$

which implies

$$\begin{aligned}\hat{z} &= \frac{1}{1 + G_{y_r,u}(G_{cz} + G_{cy}\Phi_{yz})}\hat{r} \\ &\quad - \frac{G_{y_r,u}G_{cy}\Phi_{yd} + G_{y_r,d}}{1 + G_{y_r,u}(G_{cz} + G_{cy}\Phi_{yz})}\hat{d}\end{aligned}\quad (56)$$

Let  $G_{y_r,u} = \frac{N_{y_r,u}}{D_{y_r,u}}$ ,  $G_{cz} = \frac{N_{cz}}{D_{cz}}$ , and  $G_{y_u} = \frac{N_{y_u}}{D_{y_u}}$ , and note that  $G_{y_r,d} = \frac{N_{y_r,d}}{D_{y_r,u}}$ ,  $G_{cy} = \frac{N_{cy}}{D_{cy}}$ , and  $G_{y_d} = \frac{N_{y_d}}{D_{y_u}}$ . Then

$$\Phi_{yz} = \frac{N_{y_u}N_{cz}}{D_{y_u}D_{cz} - N_{y_u}N_{cy}}, \quad \Phi_{yd} = \frac{N_{y_d}D_{cz}}{D_{y_u}D_{cz} - N_{y_u}N_{cy}}\quad (57)$$

Also, let  $\hat{r} = \frac{n_r}{d_r}$  and  $\hat{d} = \frac{n_d}{d_d}$ . Defining  $\Psi \triangleq D_{y_u}D_{cz} - N_{y_u}N_{cy}$  and  $\Gamma \triangleq D_{y_r,u}D_{cz}\Psi + N_{y_r,d}N_{cz}\Psi + N_{y_r,d}N_{cy}N_{y_u}N_{cz}$ , (56) can be written as

$$\hat{z} = \frac{D_{y_r,u}D_{cz}\Psi}{\Gamma}\hat{r} - \frac{(N_{y_r,u}N_{cy}N_{y_d} + N_{y_r,d})D_{cz}}{\Gamma}\hat{d}\quad (58)$$

Next, since (34) is an internal model of  $r$  and  $d$ , it follows that internal models of the command  $r$  and disturbance  $d$  are present in the denominator  $D_{cz}$  of  $G_{cz}$ . Therefore,  $D_{cz} = \tilde{d}_r d_r = \tilde{d}_d d_d$ , where  $\tilde{d}_r$  and  $\tilde{d}_d$  are polynomials. Hence

$$\hat{z} = \frac{D_{y_r,u}\tilde{\Psi}\tilde{d}_r n_r}{\Gamma} - \frac{(N_{y_r,u}N_{cy}N_{y_d} + N_{y_r,d}\Psi)\tilde{d}_d n_d}{\Gamma}\quad (59)$$

Assuming that  $\Gamma$  is asymptotically stable, the final value theorem implies that

$$\begin{aligned}\lim_{k \rightarrow \infty} z_k &= \lim_{z \rightarrow 1} (z-1)\hat{z} \\ &= \lim_{z \rightarrow 1} \left[ \frac{(z-1)D_{y_r,u}\tilde{\Psi}\tilde{d}_r n_r}{\Gamma} \right. \\ &\quad \left. - \frac{(z-1)(N_{y_r,u}N_{cy}N_{y_d} + N_{y_r,d}\Psi)\tilde{d}_d n_d}{\Gamma} \right] = 0\end{aligned}\quad (60)$$

### 3.4. Example 2. Output-feedback control of the two-mass system with harmonic command and harmonic disturbance

For output-feedback control of the two-mass system described in Example 1 by (31), (32), let  $y_{\text{meas}} = y_r = q_1$ , and thus  $C$  is omitted.

We consider the same harmonic command and harmonic disturbance as in Example 1. The internal model is given by the cascade of two undamped oscillators (24) whose frequencies are equal to the frequencies of the command and disturbance. Let  $x_0 = [0.2 \text{ m}, 0 \text{ m/s}, -0.1 \text{ m}, 0 \text{ m/s}]^T$ , and  $\hat{x}_{a,0} = 0$ . Let  $R_1 = I_5$ ,  $R_2 = 1$ ,  $V_1 = R_1$ ,  $V_2 = R_2$ . Let  $P_{a,0} = I_{n+n_{\text{im}}}$  and  $Q_{a,0} = I_{n+n_{\text{im}}}$ . Figure 9 shows the closed-loop response.

## 4. Application to LTV systems

For full-state-feedback and output-feedback control of LTV systems, we use the FPRE control law. Consider the discrete-time LTV system

$$x_{k+1} = A_k x_k + B_k u_k + D_{1,k} d_k\quad (61)$$

where  $A_k \in \mathbb{R}^{n \times n}$ ,  $B_k \in \mathbb{R}^n$ , and  $D_{1,k} \in \mathbb{R}^n$ . For full-state feedback, the control law is given by (7), where the constant feedback gain  $K_a$  is replaced by the time-varying feedback gain  $K_{a,k}$  given by (11), and where the constant matrices  $A$ ,  $B$  in the augmented system (5), (6) are replaced by the time-varying matrices  $A_k$ ,  $B_k$ , which results in the time-varying matrices  $A_{a,k}$ ,  $B_{a,k}$  in place of  $A_a$ ,  $B_a$  in (5), (6), (11), (12).

For output feedback, the measurement  $y_{\text{meas}}$  given by (33) is used with the FPRE control given by (11), (12) along with the augmented observer-based compensator (43), (44). The constant matrices  $A$ ,  $B$ ,  $C$  in (36), (37), (38) are replaced by the time-varying matrices  $A_k$ ,  $B_k$ ,  $C_k$ . This results in the time-varying matrices  $A_{a,k}$ ,  $B_{a,k}$ ,  $C_{a,k}$  replacing  $A_a$ ,  $B_a$ ,  $C_a$  in (11), (12), (36), (37), (38), (43), (44), and the time-varying matrices  $A_{c,k}$ ,  $B_{c,k}$ ,  $C_{c,k}$  replacing  $A_c$ ,  $B_c$ ,  $C_c$  in (45), (46), (47).

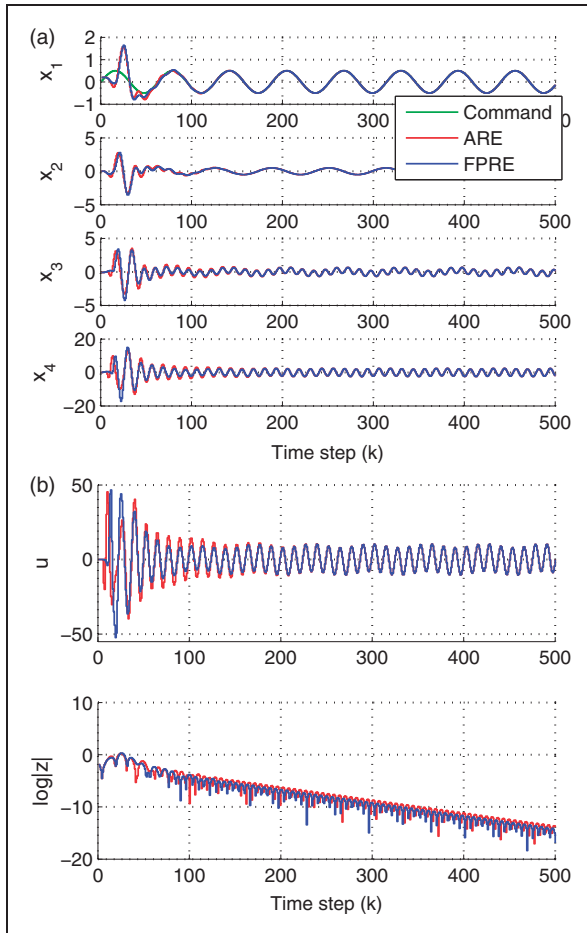


**Figure 9.** Example 2. Internal-model-based, output-feedback control of the two-mass system: (a) state trajectories; (b) control input and command-following error. The command and disturbance are harmonic with amplitudes 0.5 m and 1.0 N, respectively, and with frequencies 0.05 rad/sample and 0.5 rad/sample, respectively.

**4.1. Example 3. Command following and disturbance rejection for the Mathieu equation**

Consider the Mathieu equation Richards (1983)

$$\ddot{q} + (\alpha + \beta \cos(\omega t))q = bu \tag{62}$$

where  $\omega > 0$  is the stiffness frequency, and  $\alpha$  and  $\beta$  are real numbers. For the state vector  $x \triangleq [q \dot{q}]^T$ , the continuous-time matrices in (25) are given by

$$A_{\text{cont}}(t) = \begin{bmatrix} 0 & 1 \\ -(\alpha + \beta \cos(\omega t)) & 0 \end{bmatrix}, \quad B_{\text{cont}}(t) = \begin{bmatrix} 0 \\ b \end{bmatrix} \tag{63}$$

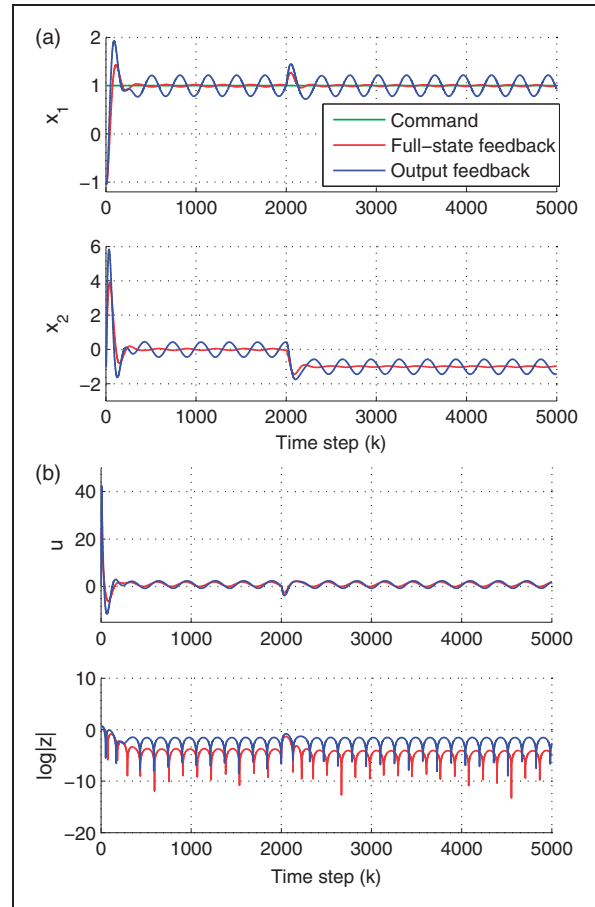


**Figure 10.** Example 3. Internal-model-based, full-state-feedback and output-feedback control of the Mathieu equation: (a) state trajectories; (b) control input and command-following error. The command and disturbance are unit steps at  $k = 0$  and  $k = 2000$ , respectively.

with the unmatched disturbance

$$D_{1,\text{cont}}(t) = \begin{bmatrix} 1 \\ 0 \end{bmatrix} \tag{64}$$

For full-state feedback, let  $y_r = q$ . For output feedback, let  $y_{\text{meas}} = y_r = q$ , and thus  $C$  is omitted. Let  $\alpha = 1$ ,  $\beta = 1$ ,  $b = 1$ ,  $\omega = 2$  rad/s, which, for  $T_s = 0.01$  s, corresponds to 0.02 rad/sample. For these parameters, the open-loop system is unstable. Let  $x_0 = [-1 \ -1]^T$ , and let  $\hat{x}_{a,0} = 0$  for output feedback.

We consider a unit step command and unit step disturbance with the integrator internal model (22). Let  $R_1 = I_3$ ,  $R_2 = 10$  for full-state feedback and output feedback, and  $V_1 = R_1$ ,  $V_2 = 1$  for output feedback. Let  $P_{a,0} = \bar{P}_a$  and  $Q_{a,0} = \bar{Q}_a$ , where  $\bar{P}_a$  and  $\bar{Q}_a$  are solutions of (10) and (42), respectively, with  $A_a = A_{a,0}$ ,  $B_a = B_{a,0}$ ,  $C_a = C_{a,0}$ , assuming that  $(A_{a,0}, B_{a,0})$  is stabilizable,  $(A_{a,0}, R_1)$  is detectable,  $(A_{a,0}, C_{a,0})$  is detectable, and  $(A_{a,0}, V_1)$  is stabilizable. Figure 10 shows that

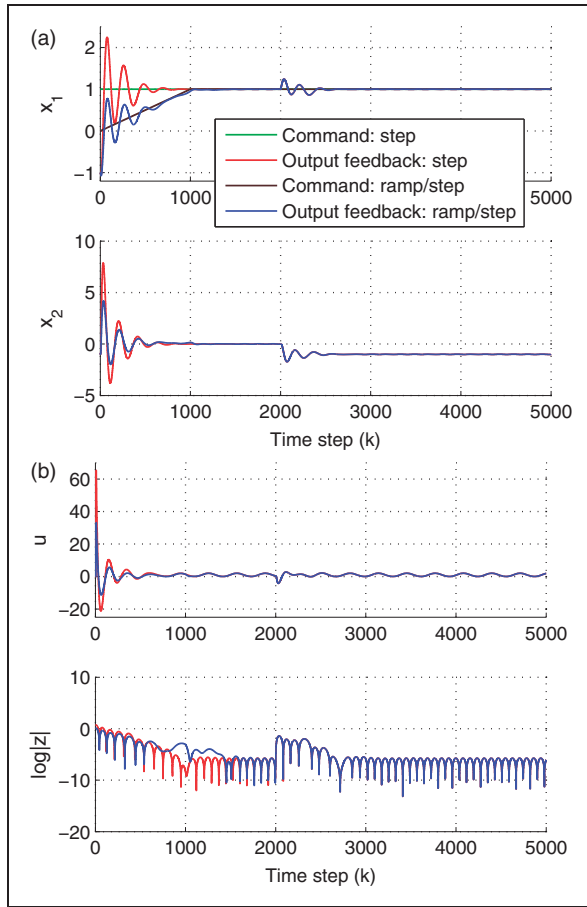


**Figure 11.** Example 3. Internal-model-based, output-feedback control of the Mathieu equation: (a) state trajectories; (b) control input and command-following error. We consider two commands at  $k=0$ : a unit step and a ramp/step. The disturbance is a unit step at  $k=2000$ . An undamped oscillator is included in the internal model to suppress oscillations due to the time-varying stiffness.

residual oscillations at the stiffness frequency are present in the response  $x_1$  for output feedback but not for full-state feedback.

To reduce the large transient values of the control input, we replace the step command with a combination of a ramp followed by a step. Let  $R_1 = I_5$ ,  $R_2 = 10^8$ ,  $V_1 = R_1$ ,  $V_2 = 1$ . Let  $P_{a,0} = \bar{P}_a$  and  $Q_{a,0} = \bar{Q}_a$ . The closed-loop response is shown in Figure 11 for the case of output feedback, where an undamped oscillator is included in the internal model to suppress residual oscillations in the response  $x_1$  due to the time-varying stiffness.

Next we add zero-mean Gaussian white noise with standard deviation 1 to the step disturbance. Open-loop responses are given in Figure 12. We consider two cases for output feedback. In the first case, the internal model is an integrator, and we let  $R_1 = I_5$ ,  $R_2 = 10$ ,  $V_1 = R_1$ ,

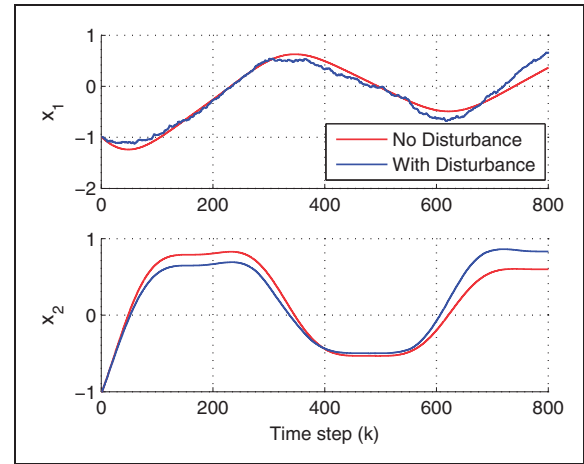


**Figure 12.** Example 3. Open-loop response of the Mathieu equation. We compare a case with no disturbance with a case where the disturbance consists of a unit step at  $k=2000$  and white noise with standard deviation 1.0.

$V_2 = 1$ ,  $P_{a,0} = \bar{P}_a$ , and  $Q_{a,0} = \bar{Q}_a$ . In the second case, the internal model is an integrator cascaded with an undamped oscillator, and we let  $R_1 = I_5$ ,  $R_2 = 10^8$ ,  $V_1 = R_1$ ,  $V_2 = 1$ ,  $P_{a,0} = \bar{P}_a$ , and  $Q_{a,0} = \bar{Q}_a$ . The closed-loop response given in Figure 13 shows that the undamped oscillator in the internal model suppresses residual oscillations in the response  $x_1$ .

Finally, we consider the previous simulation scenario, without disturbance and with zero-mean Gaussian white noise with standard deviation 0.1 added to the measurement  $y_r$ . The signal-to-noise ratio is 19.6 dB. The measurement is given in Figure 14, and the closed-loop response is given in Figure 15.

#### 4.2. Example 4. Full-state-feedback stabilization of the Mathieu equation

This example shows that FPFE may fail to stabilize an LTV system for certain choices of the state and control weightings. Consider the problem of stabilizing the Mathieu equation (62) under full-state feedback. Let  $x_0 = [1 \ 1]^T$  and  $R_1 = I_2$ . Figure 16 shows that, for  $R_2 = 0.001, 0.01, 0.05$ , the states converge to zero, whereas, for  $R_2 = 0.1$ , the states diverge.

### 5. Application to nonlinear systems

Consider the discrete-time nonlinear system

$$x_{k+1} = f(x_k, u_k) + D_1(x_k)d_k, \quad x_0 = x_0 \quad (65)$$

where  $x_k \in \mathbb{R}^n$ ,  $u_k \in \mathbb{R}$ ,  $d_k \in \mathbb{R}$ , and, for all  $x_k \in \mathbb{R}^n$  and  $u_k \in \mathbb{R}$ ,  $f(x_k, u_k) \in \mathbb{R}^n$ . We assume that (65) can be written in the state-dependent coefficient form (SDC)

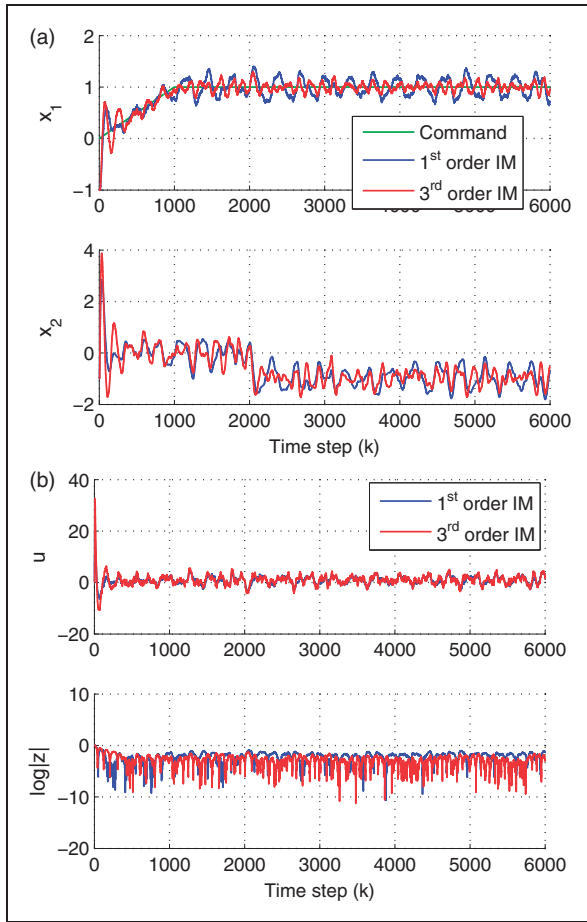


**Figure 13.** Example 3. Internal-model-based, output-feedback control of the Mathieu equation: (a) state trajectories; (b) control input and command-following error. The command is a ramp/step at  $k = 0$ . The disturbance is a unit step at  $k = 2000$  and white noise with standard deviation 1.0. The internal models are an integrator (first order) and an integrator with an undamped oscillator (third order).

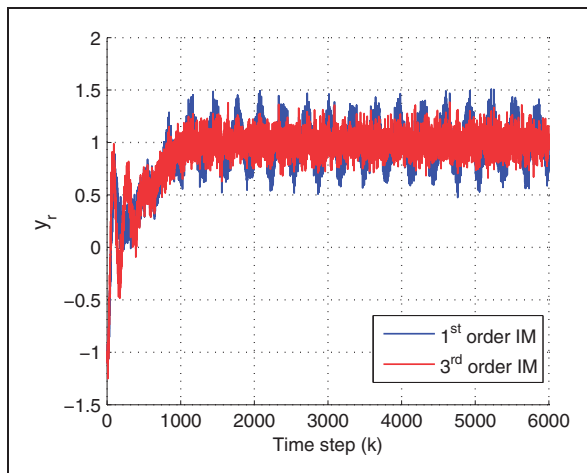


**Figure 14.** Example 3. Measurement  $y_r = q$ .

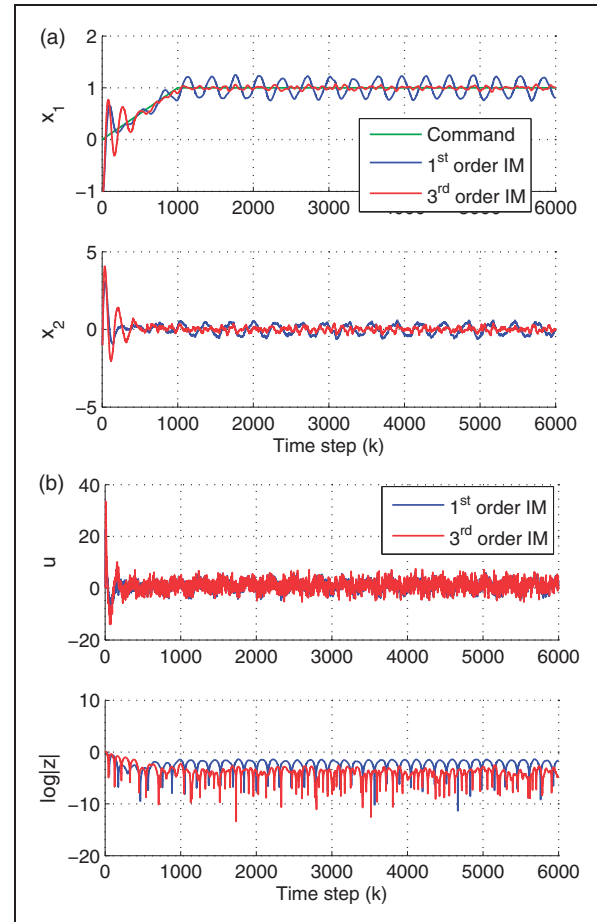


**Figure 15.** Example 3. Internal-model-based, output-feedback control of the Mathieu equation: (a) state trajectories; (b) control input and command-following error. The command is a ramp/step at  $k = 0$ , no disturbance is present, and the measurement noise is white noise with standard deviation 0.1. The internal models are an integrator (first) and an integrator with an undamped oscillator (third order).

Mracek and Cloutier (1998), Banks et al. (2007), Cimen (2010)

$$x_{k+1} = A(x_k)x_k + B(x_k)u_k + D_1(x_k)d_k \quad (66)$$

where  $A(x_k) \in \mathbb{R}^{n \times n}$ ,  $B(x_k) \in \mathbb{R}^n$ , and  $D_1(x_k) \in \mathbb{R}^n$ .

### 5.1. FPRE command following and disturbance rejection control for nonlinear systems: Full-state feedback

For internal-model-based full-state feedback, we consider the nonlinear system (65) in SDC form (66). For the command  $r$  and the output  $y_r$  given by (2), the command-following error is given by (3). For nonlinear systems, we replace the constant matrices  $A$ ,  $B$ ,  $D_1$  in the augmented system (5), (6) by the SDC matrices  $A(x_k)$ ,  $B(x_k)$ ,  $D_1(x_k)$ , which results in the SDC matrices

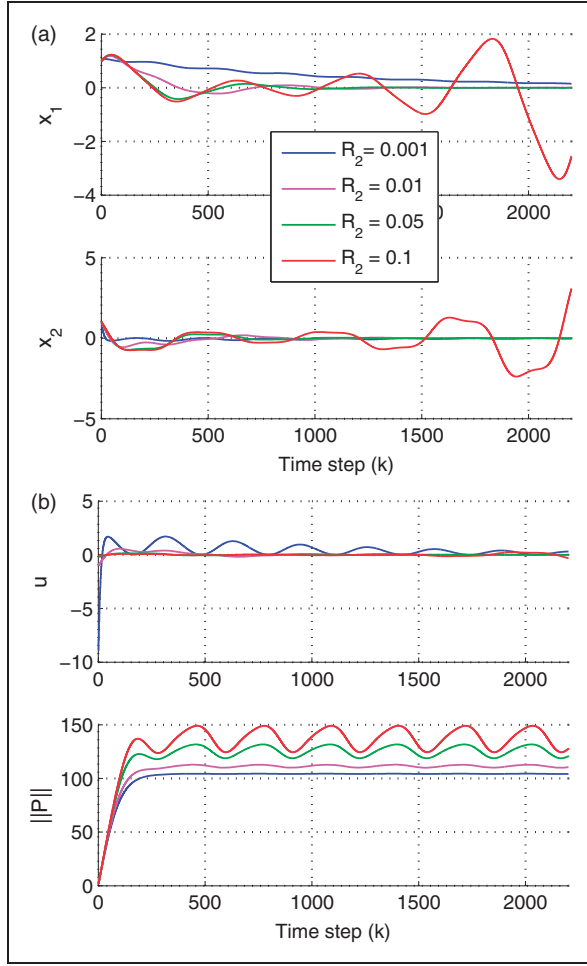


**Figure 16.** Example 4. Full-state-feedback control of the Mathieu equation for several values of  $R_2$ : (a) state trajectories; (b) control input and norm of  $P$ . For  $R_2 = 0.1$ , the states diverge.

$A_a(x_k)$ ,  $B_a(x_k)$ . Thus, the control law is given by (7) and utilizes FPRE control (11), (12) with the constant matrices  $A_a$ ,  $B_a$  replaced by the SDC matrices  $A_a(x_k)$ ,  $B_a(x_k)$ . The state and control weighting matrices  $R_1$ ,  $R_2$  in (11) and (12) can be replaced by state-dependent state and control weighting matrices  $R_1(x_k)$ ,  $R_2(x_k)$ .

### 5.2. FPRE command following and disturbance rejection control for nonlinear systems: Output feedback

In place of (65), we assume that the measurements have the form

$$y_{\text{meas},k} = h(x_k) \quad (67)$$

where  $y_{\text{meas},k} \in \mathbb{R}^m$  and  $h: \mathbb{R}^n \rightarrow \mathbb{R}^m$ . Assume that (67) can be written in the form

$$y_{\text{meas},k} = C_{\text{meas}}(x_k)x_k \quad (68)$$

where  $C_{\text{meas}}(x_k) \in \mathbb{R}^{m \times n}$ . Then, (68) can be written in the form of (33) as

$$y_{\text{meas},k} = \begin{bmatrix} y_{r,k} \\ y_k \end{bmatrix} = C_{\text{meas}}(x_k)x_k \quad (69)$$

where  $C_{\text{meas}}(x_k) = \begin{bmatrix} H \\ C(x_k) \end{bmatrix}$ ,  $H \in \mathbb{R}^{1 \times n}$ , and  $C(x_k) \in \mathbb{R}^{(m-1) \times n}$ .

Since the full state is not available, we replace the state  $x$  in the SDC matrices in (66) and (69) by its estimate  $\hat{x}$ , resulting in  $A(\hat{x})$ ,  $B(\hat{x})$ ,  $C(\hat{x})$ ,  $D_1(\hat{x})$ . If  $y_{\text{meas}}$  includes components of  $x$ , then the corresponding components of  $\hat{x}$  in the SDC's are replaced by the measurements; the modified state estimate is denoted by  $\hat{\hat{x}}$ . Then, for use in the observer-based compensator,  $A(\hat{x})$ ,  $B(\hat{x})$ ,  $C(\hat{x})$ ,  $D_1(\hat{x})$  are replaced by  $A(\hat{\hat{x}})$ ,  $B(\hat{\hat{x}})$ ,  $C(\hat{\hat{x}})$ ,  $D_1(\hat{\hat{x}})$ .

The internal-model-based output-feedback control law for nonlinear systems uses the FPRE control (11), (12) and the augmented observer-based compensator (43), (44), and is obtained using (45)–(47) with the matrices  $A$ ,  $B$ ,  $C$  in (36), (37) replaced by  $A(\hat{\hat{x}}_k)$ ,  $B(\hat{\hat{x}}_k)$ ,  $C(\hat{\hat{x}}_k)$ , the matrices  $A_a$ ,  $B_a$ ,  $C_a$  in (11), (12), (36), (37), (43), (44) replaced by  $A_a(\hat{\hat{x}}_k)$ ,  $B_a(\hat{\hat{x}}_k)$ ,  $C_a(\hat{\hat{x}}_k)$ , and the matrices  $A_c$ ,  $B_c$ ,  $C_c$  in (45), (46), (47) replaced by  $A_c(\hat{\hat{x}}_k)$ ,  $B_c(\hat{\hat{x}}_k)$ ,  $C_c(\hat{\hat{x}}_k)$ . The weighting matrices  $R_1$ ,  $R_2$ ,  $V_1$ ,  $V_2$  in (11), (12), (43) and (44) can be replaced by state-dependent weighting matrices  $R_1(\hat{\hat{x}}_k)$ ,  $R_2(\hat{\hat{x}}_k)$ ,  $V_1(\hat{\hat{x}}_k)$ ,  $V_2(\hat{\hat{x}}_k)$ .

## 6. 3. Numerical investigation of FPRE performance and robustness

In the absence of theoretical guarantees as in the case of LQG control of LTI systems, the performance of the FPRE full-state-feedback and output-feedback controllers depends strongly on the choice of the weighting matrices  $R_1$ ,  $R_2$ ,  $V_1$ ,  $V_2$ . Example 4 showed that FPRE may fail to stabilize LTV systems for some choices of the weighting matrices. Hence, the key challenge is to choose  $R_1$ ,  $R_2$  so that the solution  $P_k$  of (12) remains bounded.

In contrast to SDRE control, FPRE requires a choice of the initial condition  $P_{a,0}$  in (12). The choice  $P_{a,0} = \alpha I_{n+n_{\text{im}}}$ , where  $\alpha \geq 0$ , typically provides a convergent solution  $P_{a,k}$ . However, increasing  $\alpha$  tends to increase the transient control input  $u$ . For nonlinear systems, another convenient choice for  $P_{a,0}$  is a solution  $\bar{P}_a$  of the ARE, obtained using the SDC matrices  $A_a(x_k)$  and  $B_a(x_k)$ , which are evaluated at the initial state  $x_0$  as in SDRE; however, this choice requires that  $(A_a(x_0), B_a(x_0))$  be stabilizable. These and related issues are investigated in the following examples.

**6.1. Example 5. Command following and disturbance rejection for the Van der Pol oscillator**

Consider the Van der Pol oscillator

$$\ddot{q} - \mu(1 - q^2)\dot{q} + q = bu \quad (70)$$

where  $\mu > 0$  and  $b \neq 0$ . Define the state vector  $x \triangleq [q \dot{q}]^T$ . Equation (70) involves one nonlinear term  $-\mu x_1^2 x_2$ , which can be factored in two ways:  $-\mu x_1^2 x_2 = -(\mu x_1^2) x_2 = -(\mu x_1 x_2) x_1$ . Consequently, two SDC's can be obtained:

$$A_{1,\text{cont}}(x) = \begin{bmatrix} 0 & 1 \\ -1 & \mu(1 - x_1^2) \end{bmatrix}$$

$$A_{2,\text{cont}}(x) = \begin{bmatrix} 0 & 1 \\ -\mu x_1 x_2 & \mu \end{bmatrix}$$

Note that every affine combination  $\alpha A_{1,\text{cont}}(x) + (1 - \alpha)A_{2,\text{cont}}(x)$ , where  $\alpha$  is a real number, is also an SDC. However, we consider only the cases  $\alpha = 1$  and  $\alpha = 0$ . The control matrix is  $B_{\text{cont}} = [0 \ b]^T$ , and, for an unmatched disturbance, let  $D_1$  be given by (64). Let  $T_s = 0.01$  s, and define the corresponding discrete-time SDC's by  $A_1$  and  $A_2$ .

For full-state feedback, let  $y_r = q$ . For output feedback, let  $y_{\text{meas}} = y_r = q$ , and thus  $C$  is omitted. Let  $\mu = 0.15$ ,  $b = 1$ ,  $x_0 = [0 \ 50 \ 5]^T$ , and  $\hat{x}_{a,0} = 0$  for output feedback. We consider  $r_k = \sin(\Omega_1 k)$  and  $d_k = \cos(\Omega_2 k)$ , with  $\Omega_1 = 0.01$  rad/sample and  $\Omega_2 = 0.05$  rad/sample.

Let  $R_1 = I_6$ ,  $R_2 = 10^8$  for full-state feedback and output feedback, and let  $V_1 = R_1$ ,  $V_2 = 1$  for output feedback. Let  $P_{a,0} = P_a$  and  $Q_{a,0} = Q_a$ , where  $\bar{P}_a$  and  $\bar{Q}_a$  are solutions of (10) and (42) with the coefficients  $A_a = A_a(x_0)$ ,  $B_a = B_a(x_0)$ ,  $C_a = C_a(x_0)$ . Figures 17 and 18 show the closed-loop responses for  $A_1$  and  $A_2$  for full-state feedback and output feedback.

**6.2. Example 6. Command following and disturbance rejection for the rotational-translational actuator**

Consider the rotational-translational oscillator actuator (RTAC) (Jankovic et al., 1996; Bupp et al., 1998), shown in Figure 19. The equations of motion are given by

$$(M + m)\ddot{q} + b\dot{q} + kq = -me(\ddot{\theta} \cos \theta - \dot{\theta}^2 \sin \theta) + d \quad (71)$$

$$(J + me^2)\ddot{\theta} = -me\dot{q} \cos \theta + \tau \quad (72)$$

where  $q$  and  $\dot{q}$  are the translational position and velocity of the cart, and  $\theta$  and  $\dot{\theta}$  are the angular position and angular velocity of the rotating arm, respectively.

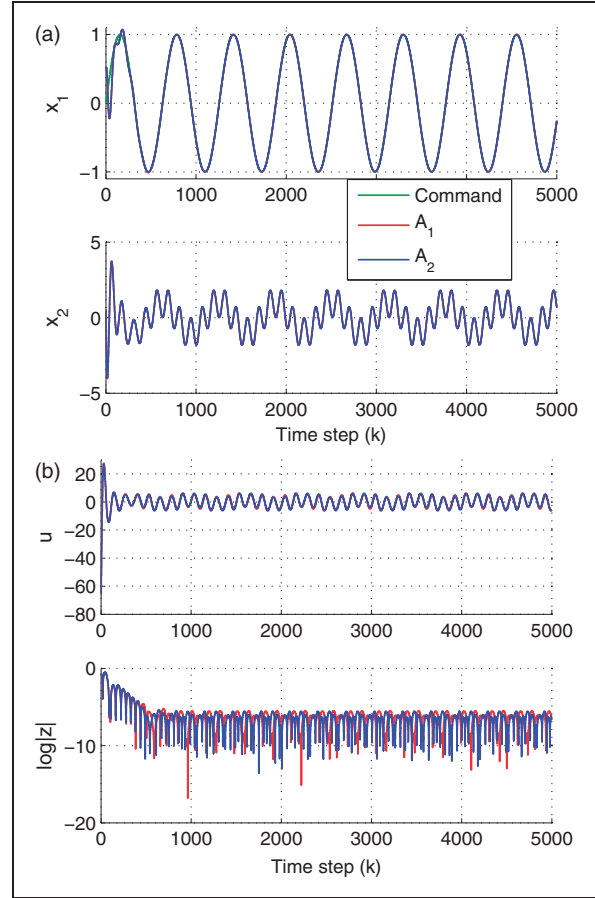


**Figure 17.** Example 5. Internal-model-based, full-state-feedback control of the Van der Pol oscillator: (a) state trajectories; (b) control input and command-following error. The command and disturbance are harmonic with unit amplitudes and with frequencies 0.01 rad/sample and 0.05 rad/sample, respectively.

$M$  is the mass of the cart,  $b$  is the damping coefficient,  $k$  is the spring stiffness,  $m$  is the mass of the proof-mass,  $J$  is the moment of inertia of the arm,  $e$  is the length of the arm,  $\tau$  is the control torque applied to the arm, and  $d$  is the disturbance force on the cart. The goal is to command the position of the cart and reject the disturbance.

For the state vector  $x = [q \dot{q} \theta \dot{\theta}]^T$ , the equations of motion have the form

$$\dot{x} = f_{\text{cont}}(x) + B_{\text{cont}}(x)\tau + D_{1,\text{cont}}(x)d \quad (73)$$

where

$$f_{\text{cont}}(x) \triangleq \begin{bmatrix} x_2 \\ -\frac{kx_1}{\delta(M+m)} - \frac{bx_2}{\delta(M+m)} + \frac{mex_4^2 \sin x_3}{\delta(M+m)} \\ x_4 \\ \frac{k\epsilon^2 x_1 \cos x_3}{\delta me} + \frac{b\epsilon^2 x_2 \cos x_3}{\delta me} - \frac{\epsilon^2 x_4^2 \sin x_3 \cos x_3}{\delta} \end{bmatrix} \quad (74)$$

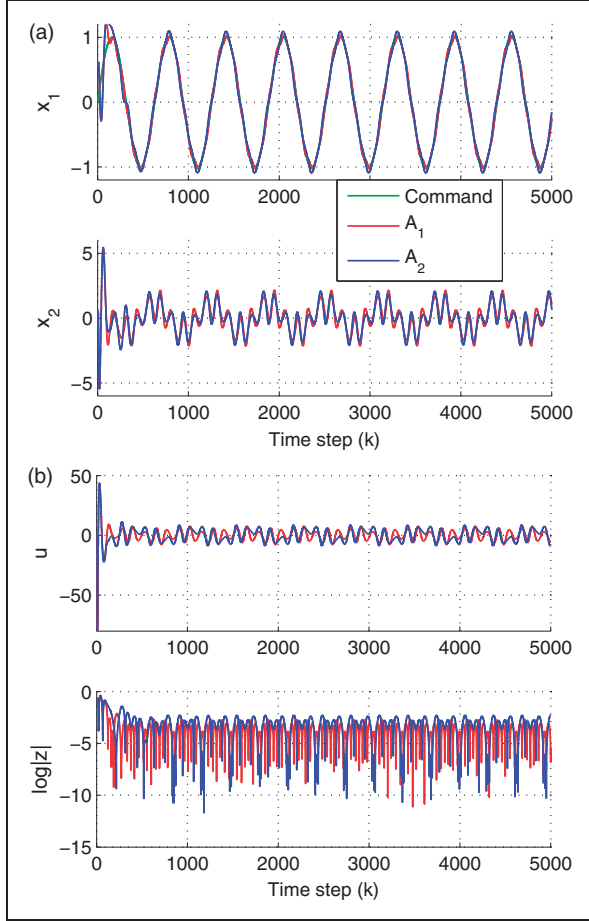


**Figure 18.** Example 5. Internal-model-based, output-feedback control of the Van der Pol oscillator: (a) state trajectories; (b) control input and command-following error. The command and disturbance are harmonic with unit amplitudes and with frequencies 0.01 rad/sample and 0.05 rad/sample, respectively.

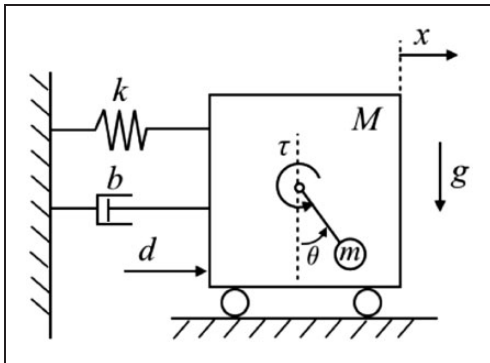


**Figure 19.** Rotational-translational actuator.

$$B_{\text{cont}}(x) \triangleq \begin{bmatrix} 0 \\ -\frac{\varepsilon^2 \cos x_3}{\delta m e} \\ 0 \\ \frac{\varepsilon^2 \cos x_3 + \delta}{\delta(J + m e^2)} \end{bmatrix}, \quad D_{1,\text{cont}}(x) \triangleq \begin{bmatrix} 0 \\ \frac{1}{\delta(M+m)} \\ 0 \\ \frac{\varepsilon^2 \cos x_3}{\delta m e} \end{bmatrix} \quad (75)$$

where

$$\varepsilon \triangleq \frac{m e}{\sqrt{(J + m e^2)(M + m)}}$$

and  $\delta \triangleq 1 - \varepsilon^2 \cos^2 x_3$ .

The vector field (74) involves four nonlinear terms that can be factored. Note that  $\frac{m e x_4^2 \sin x_3}{\delta(M+m)}$  can be factored in two ways:

$$\frac{m e x_4^2 \sin x_3}{\delta(M+m)} = \left( \frac{m e x_4 \sin x_3}{\delta(M+m)} \right) x_4 = \left( \frac{m e x_4^2 \sin x_3}{\delta(M+m) x_3} \right) x_3;$$

$$\frac{k \varepsilon^2 x_1 \cos x_3}{\delta m e}$$

can be factored in one way:

$$\frac{k \varepsilon^2 x_1 \cos x_3}{\delta m e} = \left( \frac{k \varepsilon^2 \cos x_3}{\delta m e} \right) x_1; \quad \frac{b \varepsilon^2 x_2 \cos x_3}{\delta m e}$$

can be factored in one way:

$$\frac{b \varepsilon^2 x_2 \cos x_3}{\delta m e} = \left( \frac{b \varepsilon^2 \cos x_3}{\delta m e} \right) x_2;$$

and  $\frac{\varepsilon^2 x_4^2 \sin x_3 \cos x_3}{\delta}$  can be factored in two ways:

$$\frac{\varepsilon^2 x_4^2 \sin x_3 \cos x_3}{\delta} = \left( \frac{\varepsilon^2 x_4 \sin x_3 \cos x_3}{\delta} \right) x_4$$

$$= \left( \frac{\varepsilon^2 x_4^2 \sin x_3 \cos x_3}{\delta x_3} \right) x_3.$$

Consequently, four SDC's can be obtained in this way:

$$A_{1,\text{cont}}(x) = \begin{bmatrix} 0 & 1 & 0 & 0 \\ -\frac{k}{\delta(M+m)} & -\frac{b}{\delta(M+m)} & 0 & \frac{m e x_4 \sin x_3}{\delta(M+m)} \\ 0 & 0 & 0 & 1 \\ \frac{k \varepsilon^2 \cos x_3}{\delta m e} & \frac{b \varepsilon^2 \cos x_3}{\delta m e} & 0 & -\frac{\varepsilon^2 x_4 \sin x_3 \cos x_3}{\delta} \end{bmatrix}$$

$$A_{2,\text{cont}}(x) = \begin{bmatrix} 0 & 1 & 0 & 0 \\ -\frac{k}{\delta(M+m)} & -\frac{b}{\delta(M+m)} & 0 & \frac{m e x_4 \sin x_3}{\delta(M+m)} \\ 0 & 0 & 0 & 1 \\ \frac{k \varepsilon^2 \cos x_3}{\delta m e} & \frac{b \varepsilon^2 \cos x_3}{\delta m e} & -\frac{\varepsilon^2 x_4^2 \sin x_3 \cos x_3}{\delta x_3} & 0 \end{bmatrix}$$

$$A_{3,\text{cont}}(x) = \begin{bmatrix} 0 & 1 & 0 & 0 \\ -\frac{k}{\delta(M+m)} & -\frac{b}{\delta(M+m)} & \frac{m e x_4^2 \sin x_3}{\delta(M+m) x_3} & 0 \\ 0 & 0 & 0 & 1 \\ \frac{k \varepsilon^2 \cos x_3}{\delta m e} & \frac{b \varepsilon^2 \cos x_3}{\delta m e} & 0 & -\frac{\varepsilon^2 x_4 \sin x_3 \cos x_3}{\delta} \end{bmatrix}$$

**Table 1.** RTAC parameters.

Description	Parameter	Value	Units
Cart mass	$M$	2	kg
Arm mass	$m$	0.2	kg
Arm eccentricity	$e$	0.1	m
Arm inertia	$J$	0.0002	kg-m <sup>2</sup>
Spring stiffness	$k$	200	N/m
Damping coefficient	$b$	0.4	N-s/m

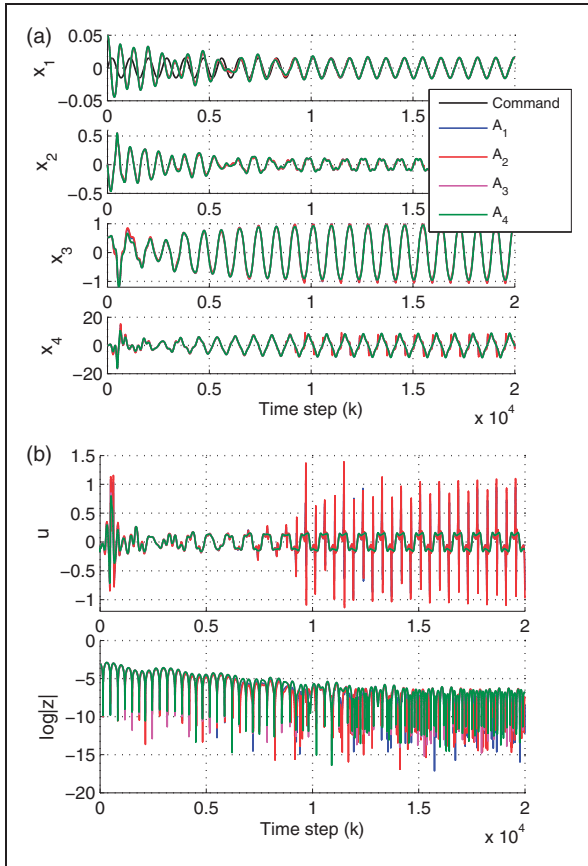


**Figure 20.** Example 6. Internal-model-based, full-state-feedback control of the RTAC: (a) state trajectories; (b) control input and command-following error. The command and disturbance are harmonic with amplitudes 0.015 m and 0.1 N, respectively, and frequency 0.007 rad/sample.

$$A_{4,\text{cont}}(x) = \begin{bmatrix} 0 & 1 & 0 & 0 \\ -\frac{k}{\delta(M+m)} & -\frac{b}{\delta(M+m)} & \frac{mex_4^2 \sin x_3}{\delta(M+m)x_3} & 0 \\ 0 & 0 & 0 & 1 \\ \frac{k\epsilon^2 \cos x_3}{\delta m\epsilon} & \frac{b\epsilon^2 \cos x_3}{\delta m\epsilon} & -\frac{\epsilon^2 x_4^2 \sin x_3 \cos x_3}{\delta x_3} & 0 \end{bmatrix}$$

Let  $T_s = 0.001$  s, and define the corresponding discrete-time SDC's by  $A_1, A_2, A_3, A_4$ . Parameters for the RTAC configuration are given in Table 1.

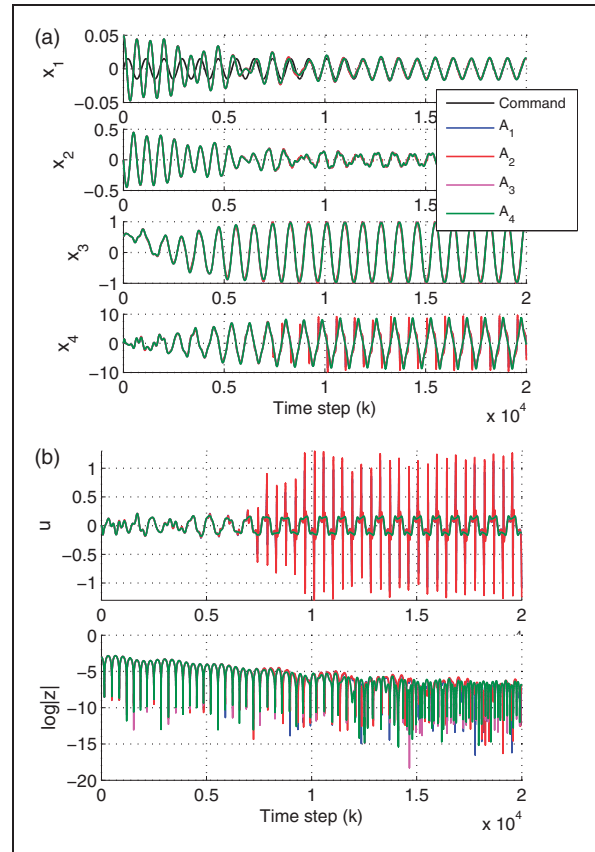


**Figure 21.** Example 6. Internal-model-based, output-feedback control of the RTAC: (a) state trajectories; (b) control input and command-following error. The command and disturbance are harmonic with amplitudes 0.015 m and 0.1 N, respectively, and frequency 0.007 rad/sample.

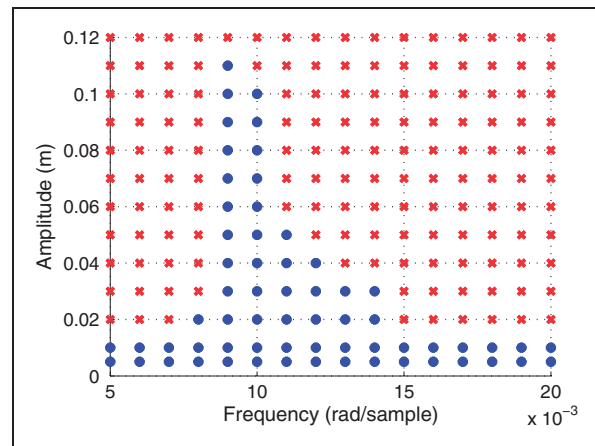


**Figure 22.** Example 6. Amplitude versus frequency for internal-model-based, output-feedback control of the RTAC. “.” denotes amplitude/frequency values for which command-following is achieved, whereas “×” denotes amplitude/frequency values for which command-following is not achieved. The results show that larger amplitudes are achievable for command frequencies near the open-loop resonance frequency of the RTAC.

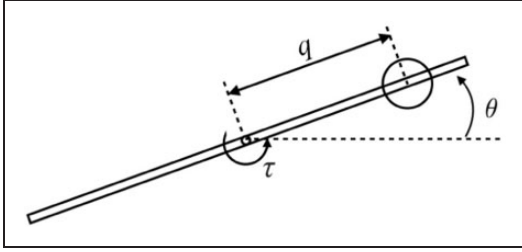


**Figure 23.** Ball and beam system.

**Table 2.** Ball and beam parameters.

Description	Parameter	Value	Units
Ball mass	$M$	0.1	kg
Ball radius	$R$	0.015	m
Beam inertia	$J$	$10^{-5}$	kg-m <sup>2</sup>
Gravitational acceleration	$g$	9.8	m/s

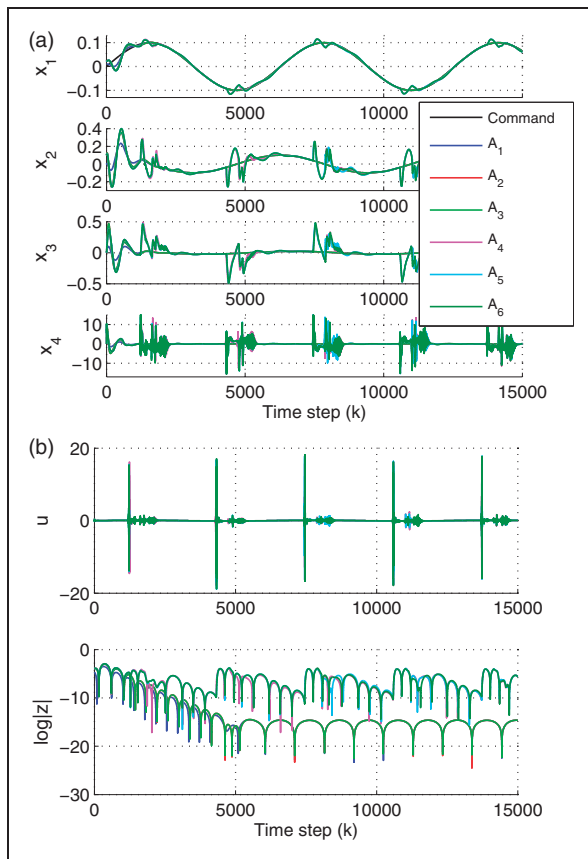


**Figure 24.** Example 7. Internal-model-based, full-state-feedback control of the ball and beam: (a) state trajectories; (b) control input and command-following error. The command and disturbance are harmonic with amplitudes 0.1 m and 0.2 N, respectively, and frequency 0.001 rad/sample. The state and control weighting matrices are  $R_1 = \text{diag}(1, 10^2 I_2, 10^4, 0.1 I_2)$  and  $R_2 = 1$ .

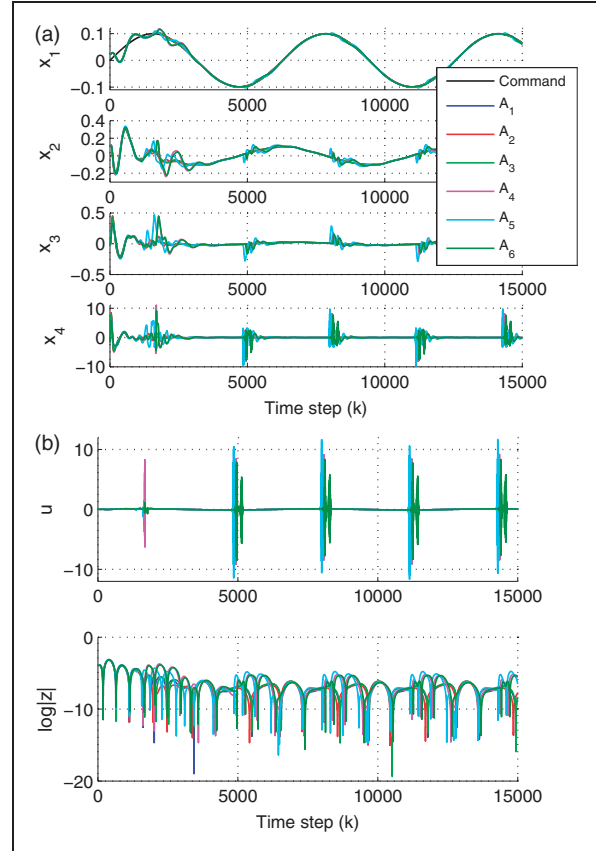


**Figure 25.** Example 7. Internal-model-based, output-feedback control of the ball and beam: (a) state trajectories; (b) control input and command-following error. The command and disturbance are harmonic with amplitudes 0.1 m and 0.2 N, respectively, and frequency 0.001 rad/sample. The weighting matrices are  $R_1 = \text{diag}(1, 10^2 I_2, 10^4, 0.1 I_2)$ ,  $R_2 = 1$ ,  $V_1 = \text{diag}(I_4, 10^4 I_2)$ ,  $V_2 = I_2$ .

The goal is to make the cart follow a harmonic trajectory in the presence of a harmonic disturbance acting on the cart. For full-state feedback and output feedback, let  $y_r = q$ . For output feedback, the cart position and arm angle are measured, that is,  $y_{\text{meas}} = [q \ \theta]^T$ , and thus  $C = [0 \ 0 \ 1 \ 0]$ . Let  $x_0 = [0.05 \text{ m}, 0 \text{ m/s}, \pi/6 \text{ rad}, 0 \text{ rad/s}]^T$ , and let  $\hat{x}_{a,0} = 0$  for output feedback.

The harmonic command  $r$  and harmonic disturbance  $d$  are given by  $r_k = 0.015 \sin(\Omega k) \text{ m}$  and  $d_k = 0.1 \cos(\Omega k) \text{ N}$ , respectively, with  $\Omega = 0.007 \text{ rad/sample}$ , which corresponds to the continuous-time frequency 7 rad/s. The damped natural frequency of the RTAC is approximately 0.01 rad/sample with a damping ratio of 8%. Let  $R_1 = \text{diag}(10^3 I_4, 10^{-3} I_2)$ ,  $R_2 = 1$  for full-state feedback and output feedback, and  $V_1 = \text{diag}(I_4, 10^4 I_2)$ ,  $V_2 = I_2$  for output feedback. Let  $P_{a,0} = I_{n+n_{im}}$  and  $Q_{a,0} = I_{n+n_{im}}$ . The responses for full-state feedback and output feedback using  $A_1, A_2, A_3, A_4$  are shown in Figures 20 and 21, respectively. Note that all SDC's provide similar state responses.

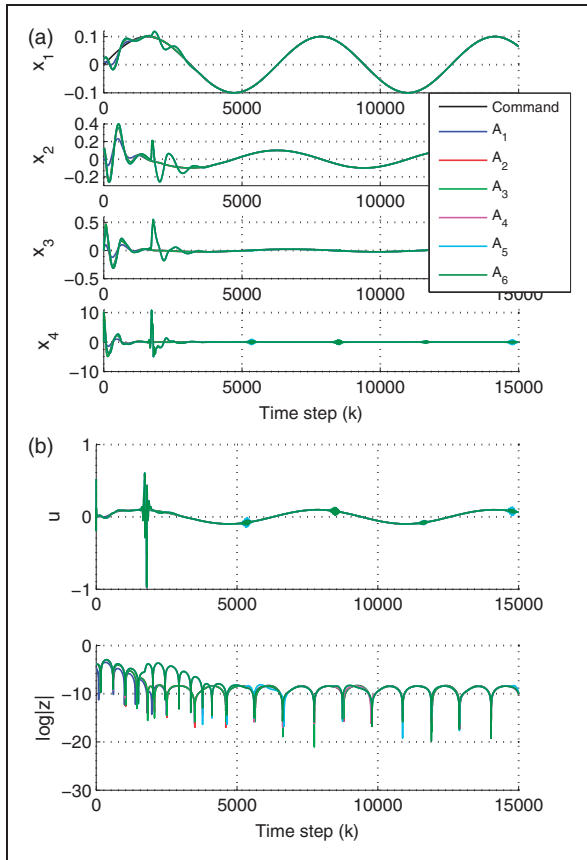


**Figure 26.** Example 7. Internal-model-based, full-state-feedback control of the ball and beam: (a) state trajectories; (b) control input and command-following error. The command and disturbance are harmonic with amplitudes 0.1 m and 0.2 N, respectively, and frequency 0.001 rad/sample. The state and control weighting matrices are  $R_1 = \text{diag}(1, 10^2 I_2, 10^4, 0.1 I_2)$  and  $R_2 = 10^5$ .

However, the control inputs for  $A_1$  and  $A_2$  exhibit oscillations with larger magnitudes than the control inputs for  $A_3$  and  $A_4$ .

To investigate the range of commandable amplitudes and frequencies in the absence of disturbances, we consider harmonic commands with amplitudes ranging within [0.005, 0.12] m and frequency ranging within [0.005, 0.02] rad/sample. Figure 22 shows the achievable amplitudes and frequencies for output feedback using SDC  $A_1$ . Note that, for command frequencies close to the undamped natural frequency of RTAC, the controller is able to follow commands with larger amplitudes.

### 6.3. Example 7. Command following and disturbance rejection for the ball and beam

The ball and beam, shown in Figure 23, consists of a symmetric beam with inertia  $J$  that rotates in a vertical

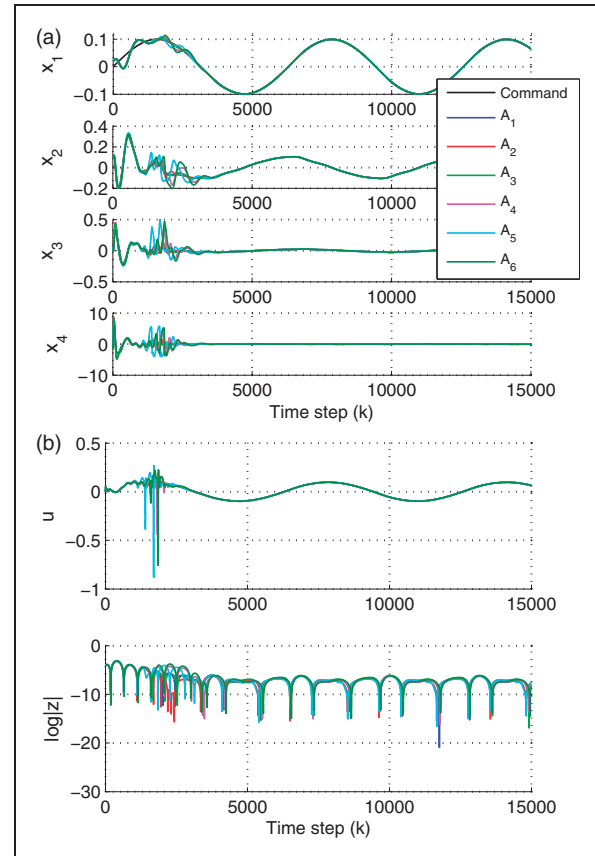


**Figure 27.** Example 7. Internal-model-based, output-feedback control of the ball and beam: (a) state trajectories; (b) control input and command-following error. The command and disturbance are harmonic with amplitudes 0.1 m and 0.2 N, respectively, and frequency 0.001 rad/sample. The weighting matrices are  $R_1 = \text{diag}(1, 10^2 I_2, 10^4, 0.1 I_2)$ ,  $R_2 = 10^5$ ,  $V_1 = \text{diag}(I_4, 10^4 I_2)$ , and  $V_2 = I_2$ .

plane subject to a torque  $\tau$ . A ball of mass  $M$  slides without friction along the beam. We are interested in using the torque  $\tau$  to control the position  $q$  of the ball along the beam.

Neglecting the inertia of the ball, the equations of motion of the ball and beam are given by Sastry (1999), Hauser et al. (1992)

$$\ddot{q} + g \sin \theta - q \dot{\theta}^2 = 0 \quad (76)$$

$$(Mq^2 + J)\ddot{\theta} + 2Mq\dot{q}\dot{\theta} + Mgq \cos \theta = \tau \quad (77)$$

For the state vector  $x \triangleq [q \quad \dot{q} \quad \theta \quad \dot{\theta}]^T$ , (76), (77) can be written as

$$\dot{x}_1 = x_2 \quad (78)$$

$$\dot{x}_2 = -g \sin x_3 + x_1 x_4^2 \quad (79)$$

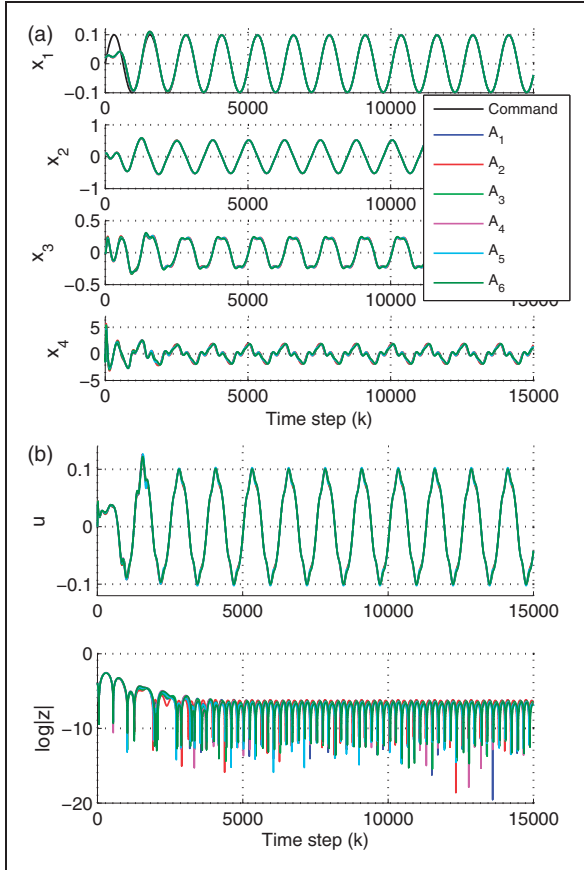


**Figure 28.** Example 7. Internal-model-based, output-feedback control of the ball and beam: (a) state trajectories; (b) control input and command-following error. The command and disturbance are harmonic with amplitudes 0.1 m and 0.2 N, respectively, and frequency 0.005 rad/sample. The weighting matrices are  $R_1 = \text{diag}(1, 10^2 I_2, 10^4, 0.1 I_2)$ ,  $R_2 = I$ ,  $V_1 = \text{diag}(I_4, 10^4 I_2)$ , and  $V_2 = I_2$ .

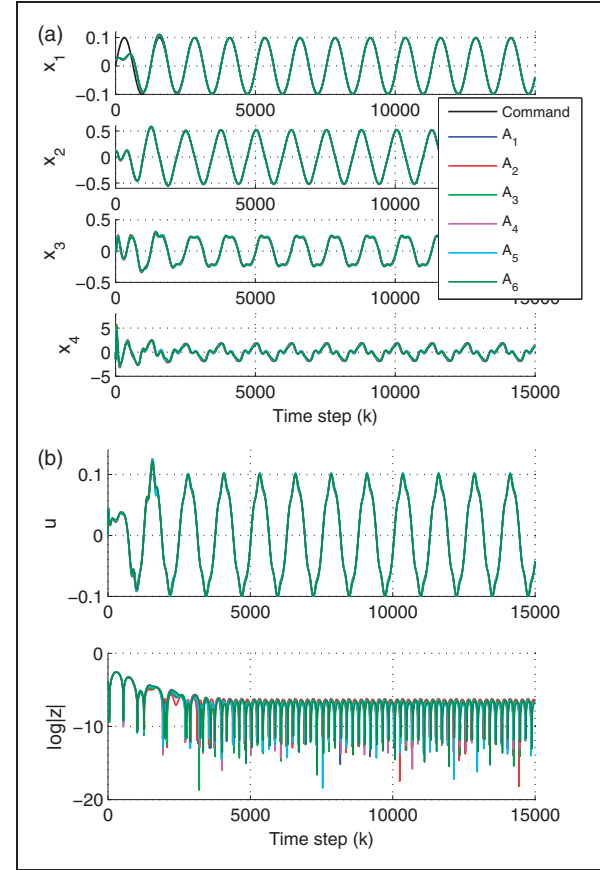


**Figure 29.** Example 7. Internal-model-based, output-feedback control of the ball and beam: (a) state trajectories; (b) control input and command-following error. The command and disturbance are harmonic with amplitudes 0.1 m and 0.2 N, respectively, and frequency 0.005 rad/sample. The weighting matrices are  $R_1 = \text{diag}(1, 10^2 I_2, 10^4, 0.1 I_2)$ ,  $R_2 = 10^5$ ,  $V_1 = \text{diag}(I_4, 10^4 I_2)$ , and  $V_2 = I_2$ .

$$\dot{x}_3 = x_4 \quad (80)$$

$$\dot{x}_4 = -\frac{2M}{Mx_1^2 + J}x_1x_2x_4 - \frac{Mg}{Mx_1^2 + J}x_1 \cos x_3 + \frac{1}{Mx_1^2 + J}\tau \quad (81)$$

The ball and beam equations (78)–(81) involve four nonlinear terms that can be factored. Note that  $\sin x_3$  can be factored in one way:  $\sin x_3 = ((\sin x_3)/x_3)x_3$ ;  $x_1x_4^2$  can be factored in two ways:  $x_1x_4^2 = (x_1x_4)x_4 = (x_4^2)x_1$ ;  $x_1x_2x_4$  can be factored in three ways:  $x_1x_2x_4 = (x_1x_2)x_4 = (x_1x_4)x_2 = (x_2x_4)x_1$ ; and  $x_2 \cos x_3$  can be factored in one way:  $x_2 \cos x_3 = (\cos x_3)x_2$ . Consequently, six SDC's can be obtained in this way:

$$A_{1,\text{cont}}(x) = \begin{bmatrix} 0 & 1 & 0 & 0 \\ x_4^2 & 0 & -\frac{g \sin x_3}{x_3} & 0 \\ 0 & 0 & 0 & 1 \\ -\frac{Mg \cos x_3 + 2Mx_2x_4}{Mx_1^2 + J} & 0 & 0 & 0 \end{bmatrix}$$

$$A_{2,\text{cont}}(x) = \begin{bmatrix} 0 & 1 & 0 & 0 \\ x_4^2 & 0 & -\frac{g \sin x_3}{x_3} & 0 \\ 0 & 0 & 0 & 1 \\ -\frac{Mg \cos x_3}{Mx_1^2 + J} & -\frac{2Mx_1x_4}{Mx_1^2 + J} & 0 & 0 \end{bmatrix}$$

$$A_{3,\text{cont}}(x) = \begin{bmatrix} 0 & 1 & 0 & 0 \\ x_4^2 & 0 & -\frac{g \sin x_3}{x_3} & 0 \\ 0 & 0 & 0 & 1 \\ -\frac{Mg \cos x_3}{Mx_1^2 + J} & 0 & 0 & -\frac{2Mx_1x_2}{Mx_1^2 + J} \end{bmatrix}$$

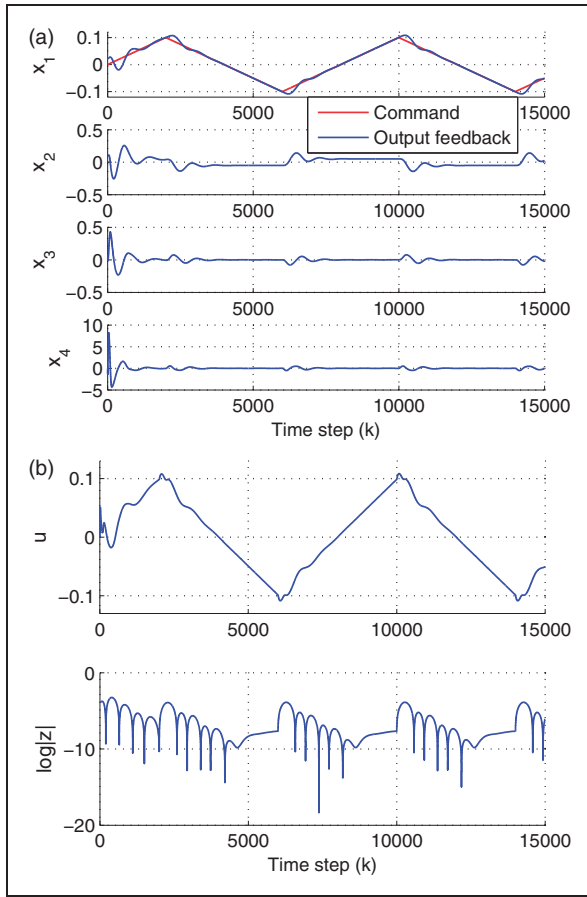


**Figure 30.** Example 7. Internal-model-based, output-feedback control of the ball and beam: (a) state trajectories; (b) control input and command-following error. The command is a triangular wave with amplitude 0.1 m, and the internal model is a double integrator.

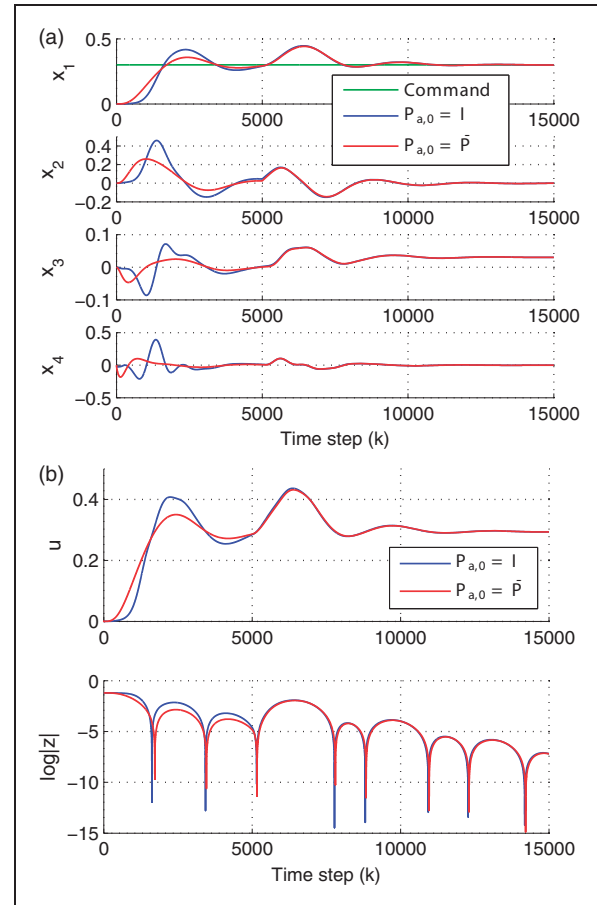


**Figure 31.** Example 8. Internal-model-based, output-feedback control of the ball and beam: (a) state trajectories; (b) control input and command-following error. The command is a step at  $k = 0$  with height 0.3 m, and the disturbance is a step with height 0.3 N at  $k = 5000$ .

$$A_{4,\text{cont}}(x) = \begin{bmatrix} 0 & 1 & 0 & 0 \\ 0 & 0 & -\frac{g \sin x_3}{x_3} & x_1 x_4 \\ 0 & 0 & 0 & 1 \\ -\frac{Mg \cos x_3 + 2Mx_2 x_4}{Mx_1^2 + J} & 0 & 0 & 0 \end{bmatrix}$$

$$A_{5,\text{cont}}(x) = \begin{bmatrix} 0 & 1 & 0 & 0 \\ 0 & 0 & -\frac{g \sin x_3}{x_3} & x_1 x_4 \\ 0 & 0 & 0 & 1 \\ -\frac{Mg \cos x_3}{Mx_1^2 + J} & -\frac{2Mx_1 x_4}{Mx_1^2 + J} & 0 & 0 \end{bmatrix}$$

$$A_{6,\text{cont}}(x) = \begin{bmatrix} 0 & 1 & 0 & 0 \\ 0 & 0 & -\frac{g \sin x_3}{x_3} & x_1 x_4 \\ 0 & 0 & 0 & 1 \\ -\frac{Mg \cos x_3}{Mx_1^2 + J} & 0 & 0 & -\frac{2Mx_1 x_2}{Mx_1^2 + J} \end{bmatrix}$$

The control matrix is  $B_{\text{cont}}(x) = [0 \ 0 \ 0 \ 1/(Mx_1^2 + J)]^T$ , and the unmatched disturbance  $D_{1,\text{cont}} = [0 \ 1 \ 0 \ 0]^T$  is applied to the ball. Let

$T_s = 0.001 \text{ s}$ , and define the corresponding discrete-time SDC's by  $A_1, A_2, A_3, A_4, A_5, A_6$ . The parameters for this system are given in Table 2.

For full-state feedback and output feedback, let  $y_r = q$ . For output feedback, the ball position and beam angle are measured, that is,  $y_{\text{meas}} = [q \ \theta]^T$ , and thus  $C = [0 \ 0 \ 1 \ 0]$ . Let  $x_0 = [0.02 \text{ m}, 0.1 \text{ m/s}, 0 \text{ rad}, 0 \text{ rad/s}]$  and  $\hat{x}_{a,0} = 0$  for output feedback. The harmonic command  $r$  and harmonic disturbance  $d$  are given by  $r_k = 0.1 \sin(\Omega k) \text{ m}$  and  $d_k = 0.2 \cos(\Omega k) \text{ N}$ , with  $\Omega = 0.001 \text{ rad/sample}$ .

Let  $R_1 = \text{diag}(1, 10^2 I_2, 10^4, 0.1 I_2)$ ,  $R_2 = 10^5$  for full-state feedback and output feedback, and  $V_1 = \text{diag}(I_4, 10^4 I_2)$ ,  $V_2 = I_2$  for output feedback. Let  $P_{a,0} = \bar{P}_a$  and  $Q_{a,0} = \bar{Q}_a$ . Figures 24 and 25 show the responses for the six SDC's for both full-state feedback and output feedback. Note that  $A_1, A_2, A_3$  provide similar performance, whereas high-frequency oscillations are present in the responses for  $A_4, A_5, A_6$ . Using  $R_2 = 10^5$ ,

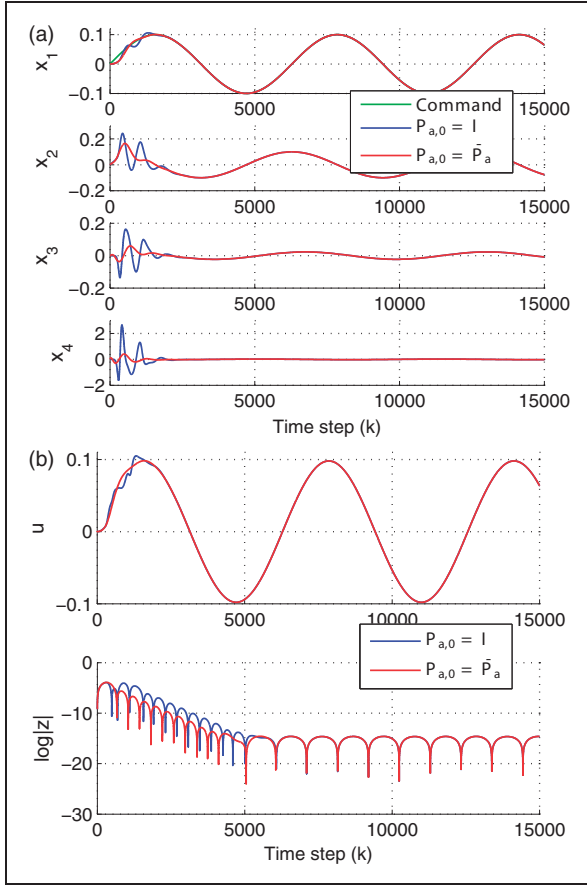


**Figure 32.** Example 8. Internal-model-based, output-feedback control of the ball and beam: (a) state trajectories; (b) control input and command-following error. The command and disturbance are harmonic with amplitudes 0.1 m and 0.2 N, respectively, and frequency 0.001 rad/sample.

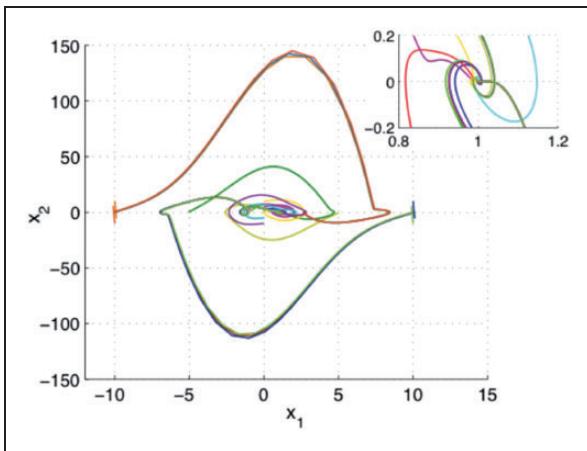


**Figure 33.** Example 9. Investigation of the domain of attraction of the Van der Pol oscillator under output-feedback control.

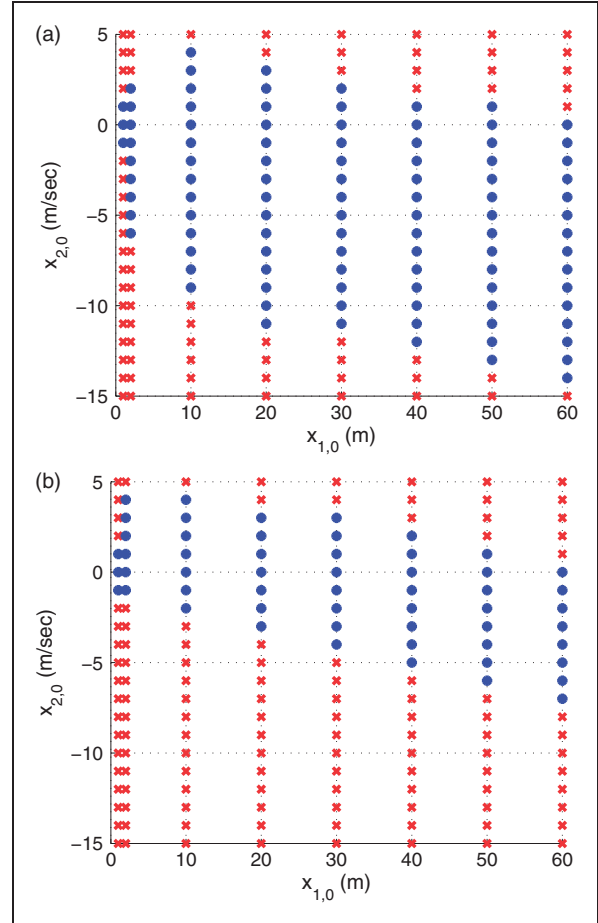


**Figure 34.** Example 10. Investigation of the domain of attraction for nonzero  $x_{1,0}$  and  $x_{2,0}$  for the ball and beam: (a) full-state feedback; (b) output feedback. “.” denotes an initial condition from which convergence is achieved, whereas “x” denotes an initial condition from which convergence is not achieved. Initial conditions with only  $x_{1,0} > 0$  are considered due to symmetry.

Figures 26 and 27 show that the high-frequency oscillations are removed, and all six SDC’s give similar responses.

Now we increase the frequency of the command and disturbance to  $\Omega = 0.005$  rad/sample. All six SDC’s give similar responses for both full-state feedback and output feedback with  $R_2 = 1$  and  $R_2 = 10^5$ . The results for output feedback are shown in Figures 28 and 29.

Next, we consider a triangular wave command with amplitude 0.1 m, and let  $d = 0$ . The internal model is the double integrator (23), and let  $R_1 = \text{diag}(1, 10^2 I_2, 10^4, 0.1 I_2)$ ,  $R_2 = 1$ ,  $V_1 = \text{diag}(I_4, 10^4 I_2)$  and  $V_2 = I_2$ . The response for output feedback with SDC  $A_1$  is shown in Figure 30.

#### 6.4. Example 8. Effect of initial condition $P_{a,0}$ for the ball and beam

To investigate the effect of the initial condition  $P_{a,0}$  on the performance of FPRE, we consider output

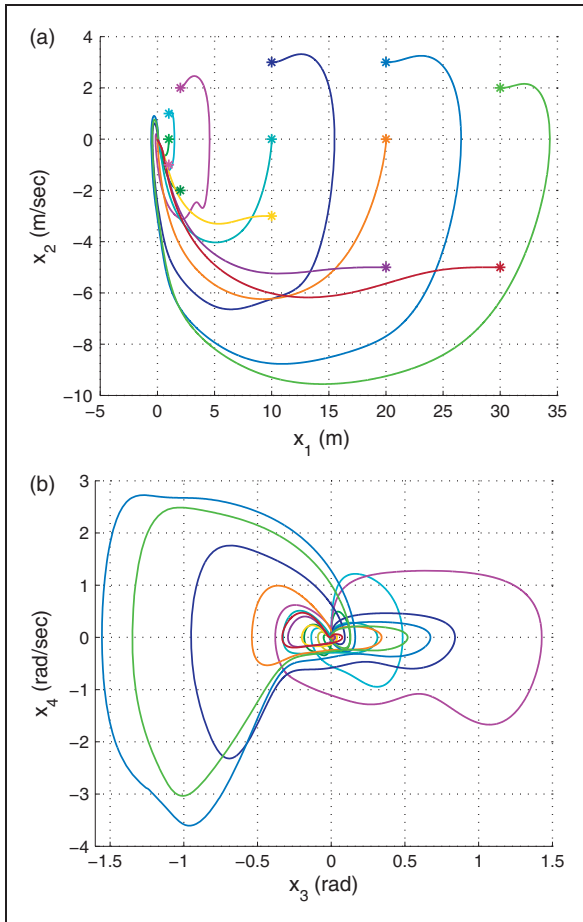


**Figure 35.** Example 10. Investigation of the domain of attraction for full-state-feedback control of the ball and beam. In (a) each dot indicates the initial ball position versus velocity, while (b) shows the beam angle versus angular velocity.

feedback as in Example 7. We compare the performance for the initial conditions  $P_{a,0} = I_{n+n_{im}}$  and  $P_{a,0} = \bar{P}_a$ , where  $\bar{P}_a$  is the solution to (10), with the coefficients  $A_a = A_a(x_0)$ ,  $B_a = B_a(x_0)$ . The weighting matrices  $R_1$ ,  $R_2$ ,  $V_1$ ,  $V_2$  are the same for both choices of  $P_{a,0}$ .

Figures 31 and 32 show that the transient response with the initial condition  $P_{a,0} = \bar{P}_a$  is better than for  $P_{a,0} = I_{n+n_{im}}$ . However, the rate of convergence is the same for both choices of the initial condition.

### 6.5. Example 9. Investigation of the domain of attraction for the Van der Pol oscillator

In this example we investigate the domain of attraction of the Van der Pol oscillator under output-feedback control. In particular, we consider a step command and step disturbance with the weighting matrices  $R_1$ ,  $R_2$ ,  $V_1$ ,  $V_2$  as given in Example 5. Figure 33 shows the phase portrait of the state trajectories for several

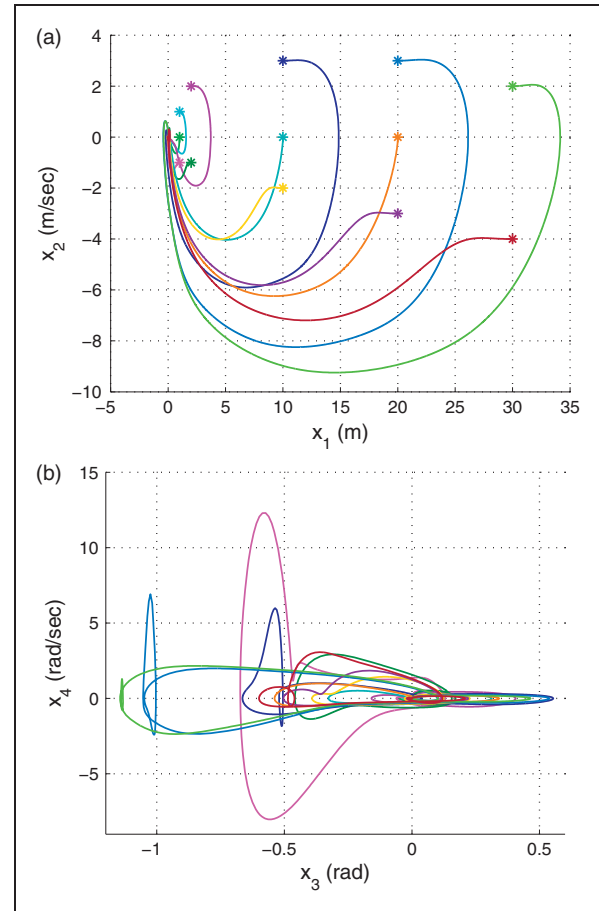


**Figure 36.** Example 10. Investigation of the domain of attraction for output-feedback control of the ball and beam using measurements of ball position and beam angle. In (a) each dot indicates the initial ball position versus velocity, while (b) shows the beam angle versus angular velocity.

initial conditions  $x_0$  contained in  $[-10, 10] \times [-10, 10]$ . Figure 33 shows that all of the state trajectories converge to  $[10]^T$ , which corresponds to zero asymptotic command-following error.

### 6.6. Example 10. Investigation of the domain of attraction for the ball and beam

In this example we estimate the domain of attraction for the ball and beam under full-state feedback and output feedback. We consider convergence to the equilibrium in the absence of a disturbance, with nonzero initial conditions on the ball position and velocity, and with zero initial conditions on the beam angle and angular velocity.

For output feedback, we assume that measurements of the ball position and beam angle are available. For all initial conditions and for both full-state feedback and output feedback, let  $R_1 = \text{diag}(10^2, 10^3 I_3)$  and  $R_2 = 10^3$ . For output feedback, let  $V_1 = I_4$ ,  $V_2 = 10^2 I_2$ ,

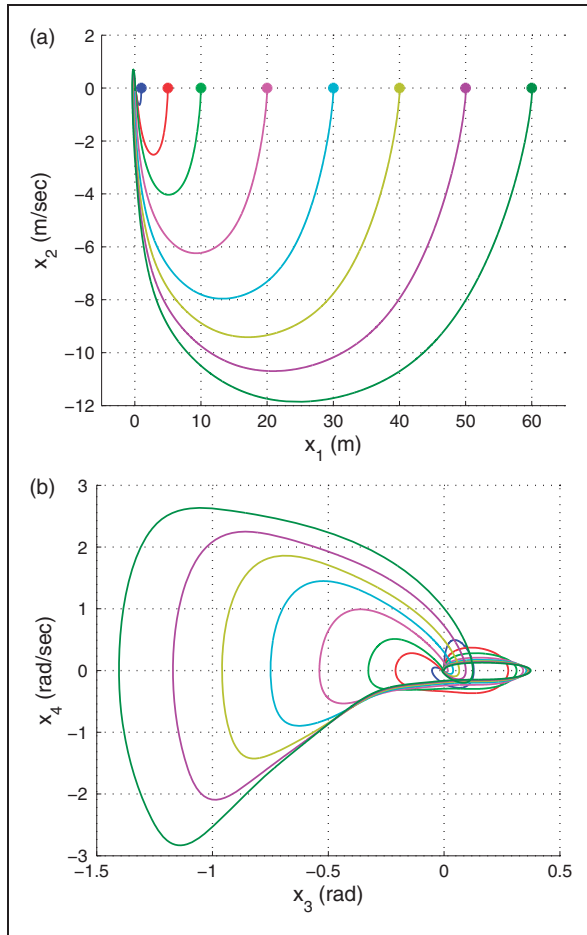


**Figure 37.** Example 10. Investigation of the domain of attraction for output-feedback control of the ball and beam using measurements of ball position only. Initial conditions with only  $x_{1,0} > 0$  are considered due to symmetry. In (a) each dot indicates the initial ball position versus velocity, while (b) shows the beam angle versus angular velocity.

and  $\hat{x}_{a,0} = [x_{1,0} \ 0 \ x_{3,0} \ 0]^T$ . Figure 34 gives a set of initial conditions with  $x_{1,0} \in [0, 60]$  m,  $x_{2,0} \in [-15, 5]$  m/s,  $x_{3,0} = 0$  rad, and  $x_{4,0} = 0$  rad/s. These values are illustrative only and are not intended to be physically meaningful. For each initial condition, Figure 34 indicates whether or not the state converges. It should be noted that the beam angle  $\theta$  satisfies  $\theta \in (-\pi/2, \pi/2)$  for all cases where the states converge. The phase portraits for selected initial conditions are shown in Figure 35 for full-state feedback, and in Figure 36 for output feedback.

Next, we consider output feedback for the case where measurements of only the ball position are available for feedback. Let  $R_1 = \text{diag}(10^2, 10^3 I_3)$ ,  $R_2 = 10^3$ ,  $V_1 = I_4$ ,  $V_2 = 100$ , and  $\hat{x}_{a,0} = [x_{1,0} \ 0 \ 0 \ 0]^T$ . We consider initial conditions with  $x_{1,0} \in [0, 60]$  m,  $x_{2,0} = 0$  m/s,  $x_{3,0} = 0$  rad, and  $x_{4,0} = 0$  rad/s. For all initial conditions within the given range, the state trajectories converge to

the zero equilibrium. The phase portraits are shown in Figure 37.

## 7. Conclusions

Output-feedback control of linear-time-varying (LTV) and nonlinear systems presents a longstanding challenge to modern control methods. Forward-propagating Riccati equation (FPRE) control addresses this problem by reversing the direction of the regulator Riccati equation and employing state-dependent coefficients (SDC's) as used by the state-dependent Riccati equation (SDRE) technique. By using an observer-based compensator structure, with state estimates used to evaluate the SDC's in the compensator in the case of nonlinear systems, FPRE provides a highly flexible technique for output-feedback control of LTV and nonlinear systems. For LTI systems, FPRE is fully justified. However, for LTV and nonlinear systems, FPRE does not guarantee stabilization. The source of the difficulty is the fact that, for LTV systems, the Lyapunov function that guarantees convergence of the state estimate may not provide an analogous Lyapunov function for the dual regulator.

FPRE provides two main advantages over the widely studied SDRE method. In particular, SDRE requires the solution of algebraic Riccati equations at each step in time, whereas FPRE requires only the time integration of these equations. Although FPRE requires an initial condition for the difference Riccati equation, we found that the initial solution of the algebraic Riccati equations often provides a suitable initial condition; for greater simplicity, the initial conditions may be taken to be a multiple of the identity matrix. The second advantage of FPRE over SDRE is the fact that solution of the algebraic Riccati equations requires stabilizability and detectability pointwise in time. These conditions may fail to be satisfied for some choices of SDC's along the trajectories of the state estimates, upon which the SDC's depend.

The contribution of this paper is an investigation of the effectiveness of FPRE on systems that have been widely studied under alternative methods, including the Mathieu equation, Van der Pol oscillator, rotational-translational actuator (RTAC), and ball and beam. The internal model principle was used in an output-feedback architecture to achieve command following and disturbance rejection for steps, ramps, and harmonics. The effect of Riccati-equation initialization, state and control weightings, domain of attraction, and choice of SDC were investigated. These examples illustrate the usefulness of FPRE in controlling these nonlinear systems under measurement constraints that are more restrictive and thus more challenging than have been considered in the prior literature. To illustrate the

potential usefulness of the method for problems of practical interest, FPRE was used to determine the range of frequencies and amplitudes of harmonic commands that can be followed by the RTAC.

The ultimate goal of this study is to motivate the development of a rigorous framework for FPRE. To further motivate this development, future work will focus on criteria for selecting the SDC as well as robustness to model uncertainty.

### Declaration of Conflicting Interests

The author(s) declared no potential conflicts of interest with respect to the research, authorship, and/or publication of this article.

### Funding

The author(s) received no financial support for the research, authorship, and/or publication of this article.

### References

- Afanas'ev VN, Kolmanovskii VB and Nosov VR (1996) *Mathematical Theory of Control Systems Design*. Netherlands: Springer.
- Arcak M (2005) Certainty-equivalence output-feedback design with circle-criterion observers. *IEEE Transactions on Automatic Control* 50(6): 905–909.
- Banks H, Lewis B and Tran H (2007) Nonlinear feedback controllers and compensators: a state-dependent Riccati equation approach. *Computational Optimization and Applications* 37(2): 177–218.
- Barbuand C, Sepulchre R, Wei L, et al. (1997) Global asymptotic stabilization of the ball-and-beam system. In: *IEEE Conference on Decision and Control*, San Diego, CA, 10–12 December 1997, pp. 2351–2355. IEEE.
- Bittanti S and Colaneri S (2009) *Periodic Systems. Filtering and Control*. London: Springer-Verlag.
- Bupp R, Bernstein D and Coppola V (1998) A benchmark problem for nonlinear control design. *International Journal of Robust and Nonlinear Control* 8(4–5): 307–310.
- Byrnes C and Isidori A (2003) Limit sets, zero dynamics, and internal models in the problem of nonlinear output regulation. *IEEE Transactions on Automatic Control* 48(10): 1712–1723.
- Byrnes C, Isidori A and Willems J (1991) Passivity, feedback equivalence, and the global stabilization of minimum phase nonlinear systems. *IEEE Transactions on Automatic Control* 36(11): 1228–1240.
- Callier F, Winkin J and Willems J (1994) Convergence of the time-invariant Riccati differential equation and LQ-problem: mechanisms of attraction. *International Journal of Control* 59(4): 983–1000.
- Chandrasekhar J, Ridley A and Bernstein D (2005) A SDRE-Based Asymptotic Observer for Nonlinear Discrete-Time Systems. In: *American Control Conference*, Portland, OR, 8–10 June, 2005, pp. 3630–3635. IEEE.
- Chen M and Kao C (1997) Control of linear time-varying systems using forward Riccati equation. *Journal of Dynamic Systems, Measurement, and Control* 119(3): 536–540.
- Cimen T (2010) Systematic and effective design of nonlinear feedback controllers via the state-dependent Riccati equation (SDRE) method. *Annual Reviews in Control* 34(1): 32–51.
- Copp DA and Hespanha JP (2014) Nonlinear output-feedback model predictive control with moving horizon estimation. In: *IEEE Conference on Decision and Control*, Los Angeles, CA, 15–17 December 2014. IEEE.
- Crassidis JL and Junkins JL (2004) *Optimal Estimation of Dynamic Systems*. CRC Press, Taylor & Francis Group, Boca Raton, FL, USA.
- Davison E and Goldenberg A (1975) Robust control of a general servomechanism problem: The servo compensator. *Automatica* 11(5): 461–471.
- Erdem E and Alleyne A (2004) Design of a class of nonlinear controllers via state dependent Riccati equations. *IEEE Transactions on Control Systems Technology* 12(1): 133–137.
- Findeisen R, Imsland L and Allgower F (2003) State and output feedback nonlinear model predictive control: An overview. *European Journal of Control* 9(2–3): 190–206.
- Forbes J and Damaren C (2010) Hybrid passivity and finite gain stability theorem: stability and control of systems possessing passivity violations. *IET Control Theory & Applications* 4(9): 1795–1806.
- Francis B and Wonham W (1975) The internal model principle for linear multivariable regulators. *Applied Mathematics and Optimization* 2(2): 170–194.
- Francis B, Sebakhy O and Wonham W (1974) Synthesis of multivariable regulators: The internal model principle. *Applied Mathematics and Optimization* 1(1): 64–86.
- Hauser J, Sastry S and Kokotovic P (1992) Nonlinear control via approximate input-output linearization: the ball and beam example. *IEEE Transactions on Automatic Control* 37(3): 392–398.
- Hoagg J, Santillo M and Bernstein D (2008) Internal model control in the shift and delta domains. *IEEE Transactions on Automatic Control* 53(4): 1066–1072.
- Isidori A (1995) *Nonlinear Control Systems*. London: Springer-Verlag.
- Isidori A, Marconi L and Serrani A (2003) *Robust Autonomous Guidance: An Internal Model Approach*. London: Springer-Verlag.
- Jankovic M, Fontaine D and Kokotovic P (1996) TORA example: cascade- and passivity-based control designs. *IEEE Transactions on Control Systems Technology* 4(3): 292–297.
- Johnson C (1971) Accommodation of external disturbances in linear regulator and servomechanism problems. *IEEE Transactions on Automatic Control* 16(6): 635–644.
- Julier S and Uhlmann J (2004) Unscented filtering and nonlinear estimation. *Proceedings of the IEEE* 92(3): 401–422.
- Khalil H (2001) *Nonlinear Systems*. Upper Saddle River, New Jersey, USA: Prentice Hall.
- Korayem M and Nekoo S (2015) State-dependent differential Riccati equation to track control of time-varying systems

- with state and control nonlinearities. *ISA Transactions* 57: 117–135.
- Mayne DQ, Raković SV, Findeisen R, et al. (2006) Robust output feedback model predictive control of constrained linear systems. *Automatica* 42(7): 1217–1222.
- Mracek C and Cloutier J (1998) Control designs for the nonlinear benchmark problem via the state-dependent Riccati equation method. *International Journal of Robust and Nonlinear Control* 8(4–5): 401–433.
- Mracek CP, Cloutier JR and D’Souza CA (1996) A new technique for nonlinear estimation. In: *IEEE International Conference on Control Applications*, Dearborn, MI, 15–18 September 1996, pp. 338–343. IEEE.
- Nijmeijer H and Fossen TI (1999) *New Directions in Nonlinear Observer Design*. London: Springer.
- Prach A, Tekinalp O and Bernstein DS (2014a) A numerical comparison of frozen-time and forward-propagating Riccati equations for stabilization of periodically time-varying systems. In: *American control conference*, Portland, OR, 4–6 June 2014, pp. 5633–5638. IEEE.
- Prach A, Tekinalp O and Bernstein DS (2014b) Faux-Riccati synthesis of nonlinear observer-based compensators for discrete-time nonlinear systems. In: *IEEE Conference on Decision and Control*, Los Angeles, CA, 15–17 December 2014, pp. 854–859. IEEE.
- Prach A, Tekinalp O and Bernstein DS (2015) Infinite-horizon linear-quadratic control by forward propagation of the differential Riccati equation. *IEEE Control Systems* 35(2): 78–93.
- Rajamani R (1998) Observers for Lipschitz nonlinear systems. *IEEE Transactions on Automatic Control* 43(3): 397–401.
- Richards JA (1983) *Analysis of Periodically Time-Varying Systems*. Berlin, Heidelberg: Springer-Verlag.
- Sastry S (1999) *Nonlinear Systems: Analysis, Stability, and Control*. New York: Springer-Verlag.
- Sauvage F, Guay M and Dochain D (2007) Design of a nonlinear finite-time converging observer for a class of nonlinear systems. *Journal of Control Science and Engineering* 2007: 1–9.
- Scherer C (2001) LPV control and full block multipliers. *Automatica* 37(3): 361–375.
- Shamma J and Athans M (1992) Gain scheduling: potential hazards and possible remedies. *IEEE Control Systems* 12(3): 101–107.
- Shamma J and Cloutier J (2003) Existence of SDRE stabilizing feedback. *IEEE Transactions on Automatic Control* 48(3): 513–517.
- Tadmor G (1992) Receding horizon revisited: An easy way to robustly stabilize an LTV system. *Systems and Control Letters* 18(4): 285–294.
- Tadmor G (2001) Dissipative design, lossless dynamics, and the nonlinear TORA benchmark example. *IEEE Transactions on Control Systems Technology* 9(2): 391–398.
- Teel AR (1992) Beyond linear feedback for the nonlinear regulator. In: *IEEE Conference on Decision and Control*, Tucson, AZ, 6–18 December 1992. IEEE.
- Teel AR (1993) Semi-global stabilization of the ‘ball and beam’ using ‘output’ feedback. In: *American control conference*, San Francisco, CA, 2–4 June 1993, pp. 2577–2581. IEEE.
- van Nieuwstadt M, Rathinam M and Murray R (1998) Differential flatness and absolute equivalence of nonlinear control systems. *SIAM Journal on Control and Optimization* 36(4): 1225–1239.
- Weiss A, Kolmanovsky I and Bernstein DS (2012) Forward-integration Riccati-based output-feedback control of linear time-varying systems. In: *American control conference*, Montreal, Canada, 27–29 June 2013, pp. 6708–6714. IEEE.
- Young P and Willems J (1972) An approach to the linear multivariable servomechanism problem. *International Journal of Control* 15(5): 961–979.